Caenorhabditis elegans locomotion dynamics is affected by internally localized magnetic fields

Eleni Gourgou[1,2,*], Yang Zhang[3,4], Ehsan Mirzakhalili[1], Bogdan Epureanu[1,+]

1. Mechanical Engineering, University of Michigan, Ann Arbor, MI, United States
2. Internal Medicine, Division of Geriatrics, Medical School, University of Michigan, Ann Arbor, MI, United States
3. Electrical Engineering and Computer Science, University of Michigan, Ann Arbor, MI, United States
4. University of Michigan and Shanghai Jiao Tong University Joint Institution, Shanghai, China

* E.G. current address: Mechanical Engineering, University of Michigan, Ann Arbor, MI, United States
+ corresponding author: Bogdan Epureanu, epureanu@umich.edu

Abstract

C. elegans with internalized magnetic nanoparticles are placed inside magnetic field to explore effects on locomotion. We hypothesize that internal magnetic fields created by nanoparticles induce localized effects on *C. elegans*' locomotion machinery. To test our hypothesis, we use young adult hermaphrodite *C. elegans* fed on *E. coli* OP50 mixed with magnetic/paramagnetic nanoparticles of 1μm, 100nm and 40nm diameter. The presence of particles inside the worms' body is verified by fluorescent and electron microscopy. A custom-made software is used to track freely moving *C. elegans* in the absence or presence of magnetic field sequentially for 200+200sec. We use established metrics to quantify locomotion-related parameters, including posture, motion and path features. Results show that key features of *C. elegans* locomotion (e.g., speed, number of bends, motion state and range) are affected by the magnetic field in worms with internalized particles, in contrast to untreated worms, which remain unaffected. Our work contributes on clarifying the magnetic field effect on *C. elegans* locomotion and introduces *C. elegans* as a potential model system to explore *in vivo* the effect of magnetic field gradient on living organisms.

Keywords

C. elegans, nanoparticles, magnetic field, locomotion

Background

The effects of magnetic field (MF) on living organisms have been a target of numerous research efforts, with their number increasing significantly during the last decades (1-3). In addition to the interest scientific community shows on the effect of alternating MF on cells (4-6), static MF effects have gained attention also (7, 8) mainly due to their correlation with activity linked to the modern way of living (9). The type of MF least studied in regard to cells is high-gradient MF. Only recent work provides the theoretical framework for the possible impact of high-gradient MF of various sources on cells' molecular components and function (10).

Model organisms have been a successful resource to study MF effects on various types of cells and tissues (11-14). Invertebrate models, like *Drosophila melanogaster*, have been used since the 80's (15-20). Interestingly, even though *C. elegans* has been an emblematic model organism to study the impact of a plethora of stimuli and environmental factors on behavior and physiology (21-25), only recently it has been used in MF related work (26-30) in which the first

animal magnetosensory neurons were identified (26). The presence of biogenic magnetite has also been reported in *C. elegans* (31).

Nanoparticles uptake by *C. elegans* worms has been a successful means to evaluate toxicity of heavy metals and pollutants (32-34), and the importance of *C. elegans* as a model system for *in vivo* nanoparticle assessment has been specifically highlighted (35). Worms' behavior (36) and locomotion (37, 38) have been evaluated under the influence of internalized metal nanoparticles. In addition, magnetized nanoparticles have been used to activate ion channels in *C. elegans* through heating (39), however only very recently internalized nanoparticles were used to locally enhance MF in the worms' body and study the subsequent impact on its metabolism (40).

C. elegans locomotion has been a major behavioral output used to investigate the impact of genetic background, environmental factors and diverse treatments on the worm's nervous system (41-46). Locomotion features have been characterized and quantified extensively and are being used as an indicator of *C. elegans* physiological status and healthspan (47-50). Therefore, locomotion is one of the first behaviors to be investigated to define whether *C. elegans* nematodes are sensitive to an environmental factor of interest.

The abovementioned scientific premises and the increasing interest in the sensitivity of *C. elegans* to MF, indicate that the investigation of MF gradient effects on worms' behavior comes at a mature point. In the present study, we use internalized magnetic nanoparticles to generate secondary MF inside the worms' body, in the closest possible proximity with tissues and cells. We use locomotion as a quantifiable and revealing behavioral expression to determine the effect of MF. Our results demonstrate a response of *C. elegans* locomotion machinery to MF gradients, and they pave the way for future studies seeking to clarify the participation of specific neurons and neuronal circuits to this still uncharacterized behavior.

Methods

Nanoparticles internalization

We investigate the locomotion of four groups of young adult N2 *C. elegans* hermaphrodites, namely worms, fed on (see Table 1):

i) plain food source *E. coli* OP50, control animals-Group C;
ii) *E. coli* OP50 mixed with 1 μm-diameter superparamagnetic particles (Dynabeads MyOne Streptavidin C1, Invitrogen, Thermo Fisher Scientific, USA), Group 1;
iii) *E. coli* OP50 mixed with 100nm-diameter iron core paramagnetic particles (nanomag-CLD-red, Micromod Partikeltechnologie GmbH, Germany), Group 100, and
iv) *E. coli* OP50 mixed with 40nm-diameter iron core paramagnetic particles (iron oxide nanocrystals, Ocean NanoTech, USA), Group 40.

In all cases, particles were isolated from the initial suspension by brief centrifugation, and were re-suspended in OP50 in a final concentration of 0.5mg/ml OP50-particle mix. Freshly made 60mm standard NGM plates were seeded with 100μl of plain OP50 or OP50-particle mix. Plates were left to dry overnight in room temperature and ~20 worms were transferred in them the next day. Nematodes were left to feed on the plain or enriched bacterial lawn for 18-20 hours, at 20°C. Then, they were either prepared for microscopy or 12-15 of them were transferred to a fresh, unseeded 35mm NGM plate for locomotion recording. In the second case, worms were left to acclimatize in the new plate for ~15min before recording. There were three reasons for transferring worms to a new, smaller plate. First, we wanted the worms to experience the effect of only internalized nanoparticles under MF and not of the remaining particles on the plate surface. Second, the presence of enriched bacterial lawn on the plate surface interfered with the tracking algorithm and could have affected the worms' locomotion due to its viscosity. Third, by using 35mm plates we decreased the distance between the electromagnets and the worms (as shown in Fig. 1), so that the worms experience a stronger external MF.

Fluorescent and Scanning Electron Microscopy (SEM)

Fluorescent Microscopy: Worms were transferred to an unseeded NGM plate and were washed with 0.5 ml of 1X PBS. Next, they were transferred to a glass slide, where they were anesthetized on fresh agar pads (51), using 10mM NaN_3 (52). Samples were imaged using a BX51WI Olympus fluorescent microscope (Olympus, Japan) coupled with an ORCA-flash4.0 camera (Hamamatsu, Japan).

Electron Microscopy: Samples were prepared as described previously (51, 53), with modifications, dissection omitted. Briefly, worms were transferred to an unseeded NGM plate and were washed with 0.5 ml of 1X PBS. Next, they were transferred to a glass cover slip and were anesthetized using 10mM NaN_3 (52). Samples were imaged using FEI Helios 650 nanolab SEM/FIB (FEI, Thermo Fisher Scientific, USA).

Worm Recording and Tracking

Recording: A 35mm plate containing worms of a specific group was placed between the two electromagnets, as shown in Fig. 1, so that the plate surface and therefore the worms were positioned close to the center of the electromagnets. First, a 200sec movie (1frame/sec) was recorded in the absence of MF (OFF state) and immediately after, a second 200sec movie (1frame/sec) was recorded with the MF on (ON state), using QCapture Pro software, (QImaging, Canada) and a Micropublisher3.3 RTV camera (QImaging, Canada), mounted on an Olympus SZ61 microscope (Olympus, Japan). The two electromagnets used were a 4.0" Dia. Electromagnet, 12 VDC, and a 3.5" Dia. Electromagnet, 12 VDC, both from APW Company, USA. Electromagnets were operated at 1.67A and 3A respectively, as indicated by the manufacturer, using a 1762 DC power supply (BK Precision Corporation, USA). By using a non-contact infrared thermometer (Omega Engineering Inc, Stamford, Ct, USA) we verified that the plate surface temperature remained constant throughout the recording period.

Tracking: Every movie was imported to MATLAB for post-processing. Each worm was tracked individually. To this end, we developed a custom tracking code in MATLAB (Fig. S2). In the first step, all frames are used to construct the movie background, which consists of all the objects that do not move for long periods of time during the entire recording. Then, each frame is subtracted from the background to extract the foreground, which consists of all moving objects. Next, the user is prompted with the initial frame of the movie, of which the background has been already subtracted, to select the worm to be tracked by the software. After the user selects the worm, the code creates a small examining frame around it and excludes the targeted worm from the rest of the movie frame. Then, the cropped figure is converted to a binary image. After the binary image is enhanced, the shape of the binary object, i.e. the worm, and its global position are stored. Next, the code proceeds to the next movie frame and uses the extracted global location of the worm as the center of the small examining frame. The small examining frame must be large enough to capture the motion of the worm in two successive movie frames. Since there is more than one worm freely moving in each experiment, there are occasions in which more than one object are included in the small examining frame. For such situations, the user is prompted by the code to manually indicate again the worm to be tracked. This way the worm that was initially selected to be tracked is always encapsulated by the examining frame. The code continues the tracking process until the last frame of the movie is processed and it stores the shape of the worm and its global location for each frame. Once finished, the user can run the code again to track another worm.

Locomotion Analysis

The following features of *C. elegans* morphology and experimental setup properties are used for the quantification of *C. elegans* locomotion parameters.

Morphology Features

1. Length: The worm length is defined as the chain-code pixel length of worm skeleton, which is converted into mm.
2. Centroid: The worm density is assumed to be constant throughout its body, so the centroid of mass is the same as geometric centroid. Since the swing of the head or tail (first or last 1/12 chain-code length part of the worm) can significantly influence centroid determination, they are ignored when computing the centroid.

Setup

1. Coordinates system: The x axis is set along the direction of the MF, between the two electromagnets, and z axis is normal to the plate, pointing upwards (Fig.1). Thus, by applying the right-hand rule, the coordinates system is established. Since we do not identify head/tail orientation for the worms, the coordinates system is important for the detection of directionality.
2. Unit Conversion: Any feature regarding length is derived first in pixels. With a known length recorded with the same experimental setup, the conversion between pixels and microns is determined.

Locomotion-related parameters of interest are divided in three categories: posture features, motion futures and path features, as described extensively by Yemini and colleagues (54), with minor modifications. A brief description of the examined features follows below.

Posture Features

1. Bends: The total body bends, measured in degrees, derive from the clockwise difference between two tangent supplementary angles (Fig. S4) along the worm skeleton. The mean value ($mean_{bends}$) and standard deviation of bends (std_{bends}) over the worm are also calculated.
2. Bend Count: This metric ($bends_{num}$) corresponds to the number of bends along a single worm. First, the supplementary angles (see above, Bends) are computed along the worm skeleton. Next, a Gaussian filter over each 1/12 of the chain-code length of the skeleton is applied to the supplementary angles to smooth out any high frequency changes, and is then normalized. The filter has a constant proportional to the reciprocal of the standard deviation, α=2.5. By checking the sequence of supplementary angles, the bend count is incremented whenever the angle reaches 0° or changes sign. The check starts from the first 1/12 segment to the last 1/12 segment to ignore small bends near the tail and the head.

Motion Features

1. Motion State: Worm's motion state can be divided in two types, the forward/backward state and the paused state. The worm is considered to be in the forward/backward state when its instantaneous speed is greater or equal to 5% of its mean length per second, and it is considered in the paused state when the instantaneous speed is less than 5% of its mean length per second. Therefore, the ratio of the time the worm is in the forward/backward state over the total recording time, namely the fb_{ratio}, and the ratio of the time the worm is in the paused state over the total recording time, namely the stay ratio $stay_{ratio}$, are calculated.
2. Velocity: Velocity is defined as the signed difference between a single worm's centroids of two sequential frames in the coordinate over the time gap between two frames (1sec). Velocity is further projected on two orthogonal axes x and y in the plane of the plate (Fig. 1), namely $velocity_x$ and $velocity_y$. The absolute value of velocity and its components give $speed$, $speed_x$ and $speed_y$, respectively.

Path Features

1. Path Curvature: This metric is defined as the angle, in radians, of the worm's path divided by the distance traveled, in microns. Three successive frames are used to

approximate the start, middle and end of the worm's instantaneous path curvature. The angle is measured by the difference in tangent angles between the second to last frame centroid and the first to the second frame centroid. Then, the path curvature is obtained by dividing the angle by the distance between the first and last centroid.

2. Range: Range is defined as the distance between the worm's centroid and the centroid of the worm's path, in each frame. The range can be projected onto the orthogonal axes x and y in the plane of the plate (Fig. 1) to obtain the x-range d_x, and the y-range d_y.

Magnetic field characterization

COMSOL Multiphysics (COMSOL Inc., MA, USA) software was used to characterize the MF that is generated by the two electromagnets in the experimental setup. The data for the magnetic flux density of the electromagnets (available from the manufacturer) was used to calibrate the parameters of the electromagnets in COMSOL Multiphysics. The COMSOL Multiphysics model was used also to estimate the intensity of the external MF, the gradient of the external MF, and the forces that are applied on magnetic particles by the external MF. MATLAB (Mathworks, MA, USA) was used to calculate the forces applied on the magnetic nanoparticles. More details are given in the Supplementary Information section.

Statistical analysis

Locomotion features were analyzed using non-parametric tests, since the Anderson-Darling normality test p-value was > 0.05 for all samples, thus rejecting the normality null hypothesis. For each metric analyzed, the Kruskal-Wallis test was used to detect whether there was any significant difference among the behaviors of all four groups in the absence of MF (OFF state). This comparison was done to determine whether the presence of particles themselves affects locomotion, regardless of external MF. Results were adjusted for ties and any difference was considered statistically significant when $p \leq 0.05$. To detect differences among worms of the same group, the Wilcoxon Signed Rank (WSR) test was used and differences were considered statistically significant when $p \leq 0.05$. All analyses were performed in Minitab (Minitab Inc., USA).

Results

Magnetic field gradient characterization

The simulation results for both electromagnets are in good agreement with the experimental results provided by the manufacturer (Fig. S1). An overview of the MF around the electromagnets and the geometry of the model in COMSOL are presented in Fig. 2A and a clear view of the MF on the plane of the worm plate surface is presented in Fig. 2B. The arrows demonstrate the direction of the MF between the two electromagnets. The contours show that the MF is stronger near the electromagnets, as expected.

We focus on the features of the MF and the forces generated on the plate surface, where the worms' locomotion takes place. The MF is almost one dimensional on the plate surface, and is stronger nearer the electromagnets (Fig. 2C). There are 9 components for the gradient of the MF. In Figure 2D, the strongest component of the MF gradient is shown (Bxx), which is parallel to x axis. The magnitude of the gradient is larger near the electromagnets.

The nanoparticles create secondary MFs in the presence of an external MF. Details on calculating the forces that are created by the particles used in the present study can be found in the Supplementary Information section. The magnitude of the MF flux is calculated in MATLAB using Eqs. [2] and [3] of Supplementary Information for configurations along the x and y axes of three nanoparticles (as shown in Fig. 3A-3D). The MF is stronger close to the particles for both configurations and decays rapidly as the distance from the particles increases (Fig. 3E). The

force between the particles in the x direction is attractive while the force between the particles in the y direction is repulsive. The attractive forces between the particles allow them to form chain-like structures, if they are not interrupted by the medium in which the particles are located (55, 56). The magnetic moment of the external MF for the particles on the worm plate surface is depicted in Fig. 3F.

Confirmation of nanoparticles uptake

Nanoparticles mixed with bacterial food were successfully internalized, as verified by microscopy methods, depending on the properties of each particle group (Fig. 4). The presence of 1μm magnetic particles (Table 1) in the worm's intestine and in the pharynx around the grinder area is verified by bright field microscopy, where the particles appear as dark (copper-colored) objects accumulated in the alimentary canal (Fig. 4A right panel), whereas control animals' intestine area appears transparent (Fig. 4A left panel). Uptake of 100nm fluorescent, magnetic particles (Table 1) was verified by fluorescent microscopy. The particles appear to accumulate along the intestine lumen and in the pharynx, as shown when filters for rhodamine, the fluorescent substance with which the particles are coated, are used (Fig. 4B). Successful feeding on 40nm magnetic particles (Table 1) is confirmed by scanning electron microscopy. As shown in Fig. 4C, when using the circular backscatter (CBS) detector, 40nm particles are visualized as white dots under the worm cuticle, in the broad area downstream of the pharynx and along the alimentary canal. The deformation of the sample due to the process followed allows for obtaining only the approximate location of the particles. The white dots which represent the particles appear in different sizes, which might be attributed to particle aggregates or to the different depth at which the particles are located.

Analysis of *C. elegans* locomotion

Analysis of selected locomotion features reveals that worms that have been fed with 1μm and 100nm diameter magnetic nanoparticles, when moving freely in MF have altered locomotion dynamics, compared to worms without internalized nanoparticles.

We examined selected posture features for each worm of each group, namely the total body bends in degrees, along with the mean bend value and the standard deviation of the bends, as well as the number of bends (bend count) realized per worm. The bends, as a feature of worms' body posture, are affected in the case of Group 1 and Group 100 worms (Figs. 5A-5D). The total body bends and the mean value of total bends are not affected by the presence of either particles or of MF (Figs. 5A, 5B). However, worms of Group 1 have significantly lower standard deviation of total body bends in the absence of MF, compared to control animals (Fig. 5C, Kruskal-Wallis test for all groups in OFF state p-value = 0.000, WSR test comparing Group C OFF and Group 1 OFF p-value = 0.000). There is also a significant difference between the number of bends per worm of Group 100 (Fig. 5D, WSR test p-value = 0.031).

Next, we analyzed features related to the motion state and velocity of the worms. The forward/backward ratio of Group 100 worms decreases when the worms are moving inside the MF (Fig. 5E, WSR test p-value = 0.010) and so does their stay ratio (Fig. 5F, WSR test p-value = 0.007). Regarding the effect of particles independently of MF, worms of Group 1 have increased stay ratio compared to control animals, even when the MF is turned off (Fig. 5F, Kruskal-Wallis test for all groups in OFF state p-value = 0.045, WSR test comparing Group C OFF and Group 1 OFF p-value = 0.005). The speed of worms fed with 100nm particles decreases when MF is on (Fig. 5K, WSR test p-value = 0.004), as does speed x for Group 100 (Fig. 5I, WSR test p-value = 0.016) and for Group 1 worms (Fig. 5I, WSR test p-value = 0.037), whereas speed y component does not change significantly for any group tested (Fig. 5J). Velocity is not affected in any of the groups tested (Fig. 5G and 5H).

We also examined two established path describing features, the path curvature and the range. The path curvature is not affected by either the presence of particles in the worm body or

by MF under the experimental conditions applied (Fig. 5L). However, the range traveled is smaller when worms of Group 1 are moving inside MF compared to the range traveled when worms of the same group are moving without the effect of MF (Fig. 5M, WSR test p-value = 0.019). This difference is not reflected in any of the distinct components of range (d_x and d_y, Figs. 5N and 5O, respectively). The p-values for all comparisons are provided in Tables S1 and S2.

Discussion

The impact of internalized nanoparticles on *C. elegans* locomotion dynamics

Metal core nanoparticles of various sizes and coatings have been used to evaluate particle toxicity using C. elegans as the subject organism (38, 57-59). Coating, size, developmental stage of the worm and duration of exposure to nanoparticles, regardless of their core material, have been shown to affect translocation of particles in various parts and tissues of the worm's body (38, 57, 60). The particles used in the present study are larger (38, 57-59) and worms have been exposed to them for a shorter period of time (18-20hrs) than in most other studies (38, 61). These differences may explain why most of the nanoparticles detected with either bright field or fluorescent microscopy (Fig. 4A, 4B) are found along the worms' pharynx, upper intestine (Fig. 4A, 4B) and lower intestine area (Fig. 4B). The location of 40nm particles in worms of Group 40 around the pharynx and grinder area (Fig. 4C) is only approximate, as some deformation has been induced on the sample during preparation, and SEM allows for detecting objects that are close to the worm's surface.

Regarding the nanoparticles' effect on locomotion, the number of body bends in C. elegans L4 larvae has been shown to significantly decrease after exposure to 9nm diameters iron oxide nanoparticles coated with organic acid for 24hrs (38). The worms used in the present work are young adults and not larvae (60, 61); larvae are developing organisms that could be more vulnerable to potential toxic effects (62). Moreover, the particles used in the present work are larger (38, 57-59), and made of different metals (37, 59), which may result in different ability to overcome the intestine barrier or translocate to other tissues, as well as to different toxicity per se. Indeed, exposure of young adults to the nanoparticles we used does not seem to massively affect posture, motion or path features (Fig. 5A-5P).

The only metrics that are affected by nanoparticles are the standard deviation of the total bends for Group 1 (Fig. 5C, comparison indicated by dashed line), and the stay ratio for Group 100 (Fig. 5F, comparison indicated by dashed line). The standard deviation of the total bends in worms of Group 1 is smaller compared to Group C (Fig. 5C), which means that Group 1 worms have a more clustered distribution of body bends amplitude around the mean. This finding might mirror an effect of 1μm particles on neurons or muscles involved in bending, which does not affect the number or the degrees of bends.

The stay ratio in worms of Group 1 (0.25, Fig. 5F) is higher compared to Group C (0.12, Fig. 5F), which means that Group 1 worms remain paused for a longer period over the total time recorded, compared to Group C. The aggregates of 1μm particles in the intestine lumen may result in heavier or more cumbersome worms, thus making it more difficult for them to move, although no difference to Group C worms speed and velocity is detected (Fig. 5G-5K). Since there is no MF present, no magnetic effect on neurons or muscles that participate in the locomotive machinery takes place (see also next section), leaving the locomotion speed unaffected. However, the weight of the particles themselves, or the friction generated between the now heavier worms and the agar surface could result in more frequent pauses.

The impact of internally localized magnetic fields on *C. elegans* locomotion dynamics

Magnetotaxis in C. elegans was recently demonstrated (26), and authors report that nematodes migrate in response to the direction of Earth's MF, with the participation of AFD

neurons, the first neurons to be identified as magnetosensory. It is suggested that endogenous magnetic material, previously reported in C. elegans, may be also involved (26, 31). In our experiments, the locomotive behavior of Group C worms, which do not contain any particles, does not seem to be affected by the externally applied MF (Fig. 5). However, the presence of 100nm and, in some cases, 1μm–diameter internalized nanoparticles has an impact on specific locomotion features (Fig. 5), when MF is applied.

Group 100 worms that are moving in MF display more body bends (Fig. 5D) and spend more time paused (Fig. 5E, 5F). More body bends possibly indicate a more W-shaped locomotion, which has been described previously in burrowing worms, as opposed to the S-shaped crawling or C-shaped swimming motion (63). Since burrowing requires the effort to move in a viscous medium, one could assume that Group 100 animals crawling in MF have to apply effort to push also their way forward, thus they integrate more bends to their locomotion. Indeed, counting the number of body bends has been suggested as a direct measure of the effort the worm is making to move (64). The assumption that moving may be laborious for these animals could be also supported by the fact that they pause more often (Fig. 5E, 5F) and they move more slowly (Fig. 5K). This is observed particularly in the direction of the MF (x direction, Fig. 2, Fig. 5I). The magnetic moment for the particles is aligned with the direction of the MF (on the plate surface they both follow the x direction, Fig. 3F).

Group 1 worms moving inside MF have also reduced speed in the direction of the MF ($speed_x$, Fig. 5I), which means that their locomotion is affected especially on the direction parallel to the MF. Group 1 worms also travel over a smaller range (Fig. 5M), when the MF is on, which could reflect a modified exploratory behavior (21, 65). This is more likely to happen due to changes in the locomotive status related to MF rather than to their incentive to explore, since other environmental factors (e.g., food abundance, temperature) do not change.

It is possible that worms slow down when they find themselves in a particular orientation inside the external MF, or when the internalized particles, which move along with the worm, obtain a particular orientation with regards to the MF. This is supported by the results presented in Fig. 2, where it is shown that the properties of MF change significantly in the direction of the MF. Therefore, any effect the MF may have on the worm or on the internalized particles is changing when a worm moves along the MF, following the direction of the MF changes themselves.

Ideally, the results shown in Figs. 2 and 3 should be combined to assess the synergistic properties of the external component of the MF (generated by the electromagnets) and of the secondary component of the MF (generated by the particles in their vicinity). However, the MF generated by the particles is very localized (in the microscale), as shown in Fig. 3. Thus, we discuss below the effects of the MF induced by the electromagnets and of the secondary MFs separately, and on their own respective scale, to explain the observed effects.

The forces that are created either by the external MF or the magnetic particles themselves are small (Fig. 3E). Such forces are not strong enough to mechanically push the worms to move along their line of action. Hence, there must be some other mechanism responsible for the detected changes in worms' locomotion. The magnitude of the external and the secondary MFs have the same order of magnitude and they are small (Fig. 2 and 3A, 3C). However, the gradient of the MF fields in the vicinity of the particles is substantially large (Fig. 2B, 2D).

Zablotskii and colleagues (10) provide several examples in which the gradient of MF can affect cellular and subcellular mechanisms in living organisms. The gradient of the secondary MF fields obtained from our simulations (up to $2x10^5$ T/m, Fig. 2B, 2D) is well above the threshold that Zablotskii and colleagues (10) suggest may impact cells with mechanosensitive ion channels (10^3T/m). The gradient of the secondary internal MF fields is also above the threshold the same authors pose for magnetically induced changes on gene expression, however we consider such a possibility highly unlikely in our case, due to the very short time the

external MF is applied (~3.5min). Therefore, the secondary field generated by the magnetic particles upon application of external MF can lead to local gradients of MF inside the worm's body, large enough to interfere with the functionality of neurons or other excitable cells (e.g., body muscle cells). This could happen by affecting the cells' ion channels, provided that the particles are very close or even in contact with the cells' membrane. Examples of *C. elegans* neurons that could be affected by internally localized MF, resulting in altered locomotion dynamics are DVA neuron, with its mechanosensitive TRPN channels (66), which is involved in body bending, and VB, VD, DB, DD motor neurons (67).

Such effects are likely to be more pronounced where the external MF is stronger, since that would result in stronger secondary MFs generated by the particles (until the magnetization of the particles becomes saturated). Hence, the locomotion of worms crawling under stronger MF, namely near the electromagnets (Fig. 2), is more likely to be affected compared to worms that are moving where the external MF is weaker. Therefore, the spatial distribution of the MF can partly explain the variations observed in the experiments. Moreover, since we have no direct control over the location where particles reside in the worms' body, the presence or absence of magnetic particles where they can affect the mechanosensitive ion channels can be another reason for the variability that we observe in our experiments.

Conclusions

The effect of internally localized secondary MF, generated by magnetic nanoparticles inside *C. elegans* body, on the dynamics of worms' locomotion is shown here for the first time. Established locomotion metrics, i.e. speed, motion state, bend count, show differences between untreated worms and worms treated with particles, moving inside magnetic field, while they show no difference between untreated and particles-treated worms. Results are supported by recent work on the effect of magnetic field gradients on cells (10, 68), mediated by magnetic nanoparticles (69). Our findings are added to the recent discoveries on *C. elegans* magnetotactic behavior (26) and are among the few available data on the *in vivo* effect of internally localized MFs (70, 71). The effect that localized MFs may have on animals' behavior and thus on the functionality of excitable cells, combined with the capability of controlling these fields by using particles of different properties, could pave the way for more detailed studies on the sensitivity of biological systems to MFs. *C. elegans* could play a key role in the effort to decipher such phenomena.

Competing Interests Statement

Authors have no competing interests.

Authors Contributions

BE and EG conceived the idea; EG, EM and BE designed the experiments; EG and YZ run experiments; YZ run tracking algorithm and processed recordings; EM created tracking algorithm and run simulations; EG, YZ and EM collected and analyzed data; EG and EM wrote the paper, with input from YZ. All authors reviewed and edited the manuscript, and gave final approval for publication.

Acknowledgments

We thank Nikos Chronis for the use of selected equipment and Syeda Maisa for her help with preliminary worm videos. We thank Jinhong Qu and Jiawei Zhang from Kenn Oldham lab for the power supply. Electron microscopy was performed at the University of Michigan Electron

Microbeam Analysis Laboratory (EMAL), with the support of University of Michigan College of Engineering; we thank John Mansfield, Kai Sun and Haiping Sun for the training.

References

1. Ghodbane S, Lahbib A, Sakly M, Abdelmelek H. Bioeffects of Static Magnetic Fields: Oxidative Stress, Genotoxic Effects, and Cancer Studies. BioMed Research International. 2013;2013:12.
2. Hong FT. Magnetic field effects on biomolecules, cells, and living organisms. Bio Systems. 1995;36(3):187-229. PubMed PMID: 8573700. Epub 1995/01/01. eng.
3. Shaw J, Boyd A, House M, Woodward R, Mathes F, Cowin G, et al. Magnetic particle-mediated magnetoreception. J R Soc Interface. 2015 Sep 6;12(110):0499. PubMed PMID: 26333810. Pubmed Central PMCID: PMC4614459.
4. Ueno S, Lövsund P, Öberg PÅ. Effects of alternating magnetic fields and low-frequency electric currents on human skin blood flow. Medical and Biological Engineering and Computing. 1986 January 01;24(1):57-61.
5. Öcal Il, Kalkan T, GÃ¼nay s. Effects of alternating magnetic field on the metabolism of the healthy and diabetic organisms. Brazilian Archives of Biology and Technology. 2008;51:523-30.
6. Belova NA, Acosta-Avalos D. The Effect of Extremely Low Frequency Alternating Magnetic Field on the Behavior of Animals in the Presence of the Geomagnetic Field. Journal of Biophysics. 2015;2015:8.
7. Miyakoshi J. Effects of static magnetic fields at the cellular level. Progress in biophysics and molecular biology. 2005 Feb-Apr;87(2-3):213-23. PubMed PMID: 15556660. Epub 2004/11/24. eng.
8. Teodori L, Grabarek J, Smolewski P, Ghibelli L, Bergamaschi A, De Nicola M, et al. Exposure of cells to static magnetic field accelerates loss of integrity of plasma membrane during apoptosis. Cytometry. 2002;49(3):113-8.
9. Lewczuk B, Redlarski G, #x17b, ak A, Zi, #xf3, et al. Influence of Electric, Magnetic, and Electromagnetic Fields on the Circadian System: Current Stage of Knowledge. BioMed Research International. 2014;2014:13.
10. Zablotskii V, Polyakova T, Lunov O, Dejneka A. How a High-Gradient Magnetic Field Could Affect Cell Life. 2016 11/18/online;6:37407.
11. Osipova EA, Pavlova VV, Nepomnyashchikh VA, Krylov VV. Influence of magnetic field on zebrafish activity and orientation in a plus maze. Behavioural processes. 2016 Jan;122:80-6. PubMed PMID: 26589739. Epub 2015/11/22. eng.
12. Shcherbakov D, Winklhofer M, Petersen N, Steidle J, Hilbig R, Blum M. Magnetosensation in zebrafish. Current Biology.15(5):R161-R2.
13. Malkemper EP, Eder SHK, Begall S, Phillips JB, Winklhofer M, Hart V, et al. Magnetoreception in the wood mouse (Apodemus sylvaticus): influence of weak frequency-modulated radio frequency fields. 2015 04/29/online;5:9917.
14. Kumari K, Capstick M, Cassara AM, Herrala M, Koivisto H, Naarala J, et al. Effects of intermediate frequency magnetic fields on male fertility indicators in mice. Environmental Research. 2017 2017/08/01/;157:64-70.
15. Fedele G, Green EW, Rosato E, Kyriacou CP. An electromagnetic field disrupts negative geotaxis in Drosophila via a CRY-dependent pathway. 2014 07/14/online;5:4391.
16. Naito M, Hirai S, Mihara M, Terayama H, Hatayama N, Hayashi S, et al. Effect of a Magnetic Field on Drosophila under Supercooled Conditions. PLoS ONE. 2012 12/28 06/20/received 11/12/accepted;7(12):e51902. PubMed PMID: PMC3532350.
17. Ramirez E, Monteagudo JL, Garcia-Gracia M, Delgado JMR. Oviposition and development of Drosophila modified by magnetic fields. Bioelectromagnetics. 1983;4(4):315-26.

18. Kale PG, Baum JW. Genetic effects of strong magnetic fields in drosophila melanogaster: II. Lack of interaction between homogeneous fields and fission neutron-plus-gamma radiation. Environmental Mutagenesis. 1980;2(2):179-86.
19. Bae J-E, Bang S, Min S, Lee S-H, Kwon S-H, Lee Y, et al. Positive geotactic behaviors induced by geomagnetic field in Drosophila. Molecular Brain. 2016 May 18;9(1):55.
20. Giachello CNG, Scrutton NS, Jones AR, Baines RA. Magnetic Fields Modulate Blue-Light-Dependent Regulation of Neuronal Firing by Cryptochrome. The Journal of Neuroscience. 2016;36(42):10742-9.
21. Cheung BH, Cohen M, Rogers C, Albayram O, de Bono M. Experience-dependent modulation of C. elegans behavior by ambient oxygen. Curr Biol. 2005 May 24;15(10):905-17. PubMed PMID: 15916947. Epub 2005/05/27. eng.
22. de Bono M, Bargmann CI. Natural Variation in a Neuropeptide Y Receptor Homolog Modifies Social Behavior and Food Response in C. elegans. Cell. 1998 9/4/;94(5):679-89.
23. Liedtke W, Tobin DM, Bargmann CI, Friedman JM. Mammalian TRPV4 (VR-OAC) directs behavioral responses to osmotic and mechanical stimuli in Caenorhabditis elegans. Proceedings of the National Academy of Sciences. 2003 November 25, 2003;100(suppl 2):14531-6.
24. Hedgecock EM, Russell RL. Normal and mutant thermotaxis in the nematode Caenorhabditis elegans. Proc Natl Acad Sci U S A. 1975 Oct;72(10):4061-5. PubMed PMID: 1060088. Pubmed Central PMCID: PMC433138. Epub 1975/10/01. eng.
25. Ward A, Liu J, Feng Z, Shawn Xu XZ. Light-sensitive neurons and channels mediate phototaxis in C. elegans. Nature neuroscience. 2008 07/06;11(8):916-22. PubMed PMID: PMC2652401.
26. Vidal-Gadea A, Ward, K., Beron, C., Ghorashian, N., Gokce, S., Russell, J., Truong, N., Parikh, A., Gadea, O., Ben-Yakar, A., Pierce-Shimomura, J. Magnetosensitive neurons mediate geomagnetic orientation in Caenorhabditis elegans. Elife. 2015 Jun 17;4. PubMed PMID: 26083711. Pubmed Central PMCID: PMC4525075.
27. Njus Z, Feldmann D, Brien R, Kong T, Kalwa U, Pandey S. Characterizing the Effect of Static Magnetic Fields on <i>C. elegans</i> Using Microfluidics. Advances in Bioscience and Biotechnology. 2015;06(09):583-91.
28. Long X, Ye J, Zhao D, Zhang S-J. Magnetogenetics: remote non-invasive magnetic activation of neuronal activity with a magnetoreceptor. Science Bulletin. 2015 2015/12/01/;60(24):2107-19.
29. Wang L, Du H, Guo X, Wang X, Wang M, Wang Y, et al. Developmental abnormality induced by strong static magnetic field in Caenorhabditis elegans. Bioelectromagnetics. 2015;36(3):178-89.
30. Lee C-H, Hung Y-C, Huang GS. Static magnetic field accelerates aging and development in nematode. Communicative & Integrative Biology. 2010 Nov-Dec 11/01 06/18/received 06/18/accepted;3(6):528-9. PubMed PMID: PMC3038054.
31. Cranfield CG, Dawe A, Karloukovski V, Dunin-Borkowski RE, de Pomerai D, Dobson J. Biogenic magnetite in the nematode caenorhabditis elegans. Proc Biol Sci. 2004 Dec 7;271 Suppl 6:S436-9. PubMed PMID: 15801597. Pubmed Central PMCID: PMC1810097.
32. Khare P, Sonane M, Pandey R, Ali S, Gupta KC, Satish A. Adverse Effects of TiO2 and ZnO Nanoparticles in Soil Nematode, Caenorhabditis elegans. Journal of Biomedical Nanotechnology. 2011 //;7(1):116-7.
33. Meyer JN, Lord CA, Yang XY, Turner EA, Badireddy AR, Marinakos SM, et al. Intracellular uptake and associated toxicity of silver nanoparticles in Caenorhabditis elegans. Aquatic toxicology (Amsterdam, Netherlands). 2010 Oct 15;100(2):140-50. PubMed PMID: 20708279. Epub 2010/08/17. eng.
34. Kim JH, Lee SH, Cha YJ, Hong SJ, Chung SK, Park TH, et al. C. elegans-on-a-chip for in situ and in vivo Ag nanoparticles' uptake and toxicity assay. 2017 01/09/online;7:40225.

35. Gonzalez-Moragas L, Roig A, Laromaine A. C. elegans as a tool for in vivo nanoparticle assessment. Advances in Colloid and Interface Science. 2015 2015/05/01/;219:10-26.
36. Ma H, Bertsch PM, Glenn TC, Kabengi NJ, Williams PL. Toxicity of manufactured zinc oxide nanoparticles in the nematode Caenorhabditis elegans. Environmental toxicology and chemistry. 2009 Jun;28(6):1324-30. PubMed PMID: 19192952. Epub 2009/02/06. eng.
37. Li Y, Yu S, Wu Q, Tang M, Pu Y, Wang D. Chronic Al2O3-nanoparticle exposure causes neurotoxic effects on locomotion behaviors by inducing severe ROS production and disruption of ROS defense mechanisms in nematode Caenorhabditis elegans. Journal of hazardous materials. 2012 Jun 15;219-220:221-30. PubMed PMID: 22521136. Epub 2012/04/24. eng.
38. Wu Q, Li Y, Tang M, Wang D. Evaluation of Environmental Safety Concentrations of DMSA Coated Fe(2)O(3)-NPs Using Different Assay Systems in Nematode Caenorhabditis elegans. PLoS ONE. 2012 08/17 05/31/received 07/23/accepted;7(8):e43729. PubMed PMID: PMC3422352.
39. Huang H, Delikanli S, Zeng H, Ferkey DM, Pralle A. Remote control of ion channels and neurons through magnetic-field heating of nanoparticles. Nat Nanotechnol. 2010 Aug;5(8):602-6. PubMed PMID: 20581833.
40. Wang L, Wang M, Du H, Liu Y, Xu A. Lipid Metabolism was Interfered by Phosphatidylcholine-Coated Magnetic Nanoparticles in C. elegans Exposed to 0.5 T Static Magnetic Field. Journal of Nanoscience and Nanotechnology. 2017 //;17(5):3172-80.
41. Gourgou E, Chronis, N. Chemically induced oxidative stress affects ASH neuronal function and behavior in C. elegans. Scientific Reports. 2016 12/06/online;6:38147.
42. Li G, Gong J, Lei H, Liu J, Xu XZS. Promotion of behavior and neuronal function by reactive oxygen species in C. elegans. Nature Communications. 2016 11/08/online;7:13234.
43. Liu J, Zhang, B., Lei, H., Feng, Z., Liu, J., Hsu, A. L., Xu, X. Z. Functional aging in the nervous system contributes to age-dependent motor activity decline in C. elegans. Cell metabolism. 2013 Sep 3;18(3):392-402. PubMed PMID: 24011074. Pubmed Central PMCID: PMC3811915. Epub 2013/09/10. Eng.
44. Hsu A-L, Feng Z, Hsieh M-Y, Xu XZS. Identification by machine vision of the rate of motor activity decline as a lifespan predictor in C. elegans. Neurobiology of aging. 2009 02/05;30(9):1498-503. PubMed PMID: PMC2747634.
45. Parida L, Neogi S, Padmanabhan V. Effect of Temperature Pre-Exposure on the Locomotion and Chemotaxis of C. elegans. PLOS ONE. 2014;9(10):e111342.
46. Pierce-Shimomura JT, Chen BL, Mun JJ, Ho R, Sarkis R, McIntire SL. Genetic analysis of crawling and swimming locomotory patterns in C. elegans. Proceedings of the National Academy of Sciences of the United States of America. 2008 12/12 04/19/received;105(52):20982-7. PubMed PMID: PMC2634943.
47. Bansal A, Zhu LJ, Yen K, Tissenbaum HA. Uncoupling lifespan and healthspan in Caenorhabditis elegans longevity mutants. Proceedings of the National Academy of Sciences. 2015 January 20, 2015;112(3):E277-E86.
48. Shtonda BB, Avery L. Dietary choice behavior in Caenorhabditis elegans. The Journal of experimental biology. 2006;209(Pt 1):89-102. PubMed PMID: PMC1352325.
49. Peliti M, Chuang JS, Shaham S. Directional Locomotion of C. elegans in the Absence of External Stimuli. PLOS ONE. 2013;8(11):e78535.
50. Hahm J-H, Kim S, DiLoreto R, Shi C, Lee S-JV, Murphy CT, et al. C. elegans maximum velocity correlates with healthspan and is maintained in worms with an insulin receptor mutation. 2015 11/20/online;6:8919.
51. Shaham SW. Methods in Cell Biology, WormBook. 2006. In: WormBook : the online review of C elegans biology [Internet]. Available from: http://www.wormbook.org.

52. Sulston JE HJ. Methods. In: WB W, editor. The Nematode Caenorhabditis elegans. Cold Spring Harbor, NY: Cold Spring Harbor Laboratory Press; 1988. p. 587–606.
53. Hall DH, Winfrey VP, Blaeuer G, Hoffman LH, Furuta T, Rose KL, et al. Ultrastructural Features of the Adult Hermaphrodite Gonad of Caenorhabditis elegans: Relations between the Germ Line and Soma. Developmental Biology. 1999 8/1/;212(1):101-23.
54. Yemini E, Jucikas T, Grundy LJ, Brown AEX, Schafer WR. A database of C. elegans behavioral phenotypes. Nature methods. 2013 07/14;10(9):877-9. PubMed PMID: PMC3962822.
55. Mirzakhalili E, Nam W, Epureanu BI. Reduced-order models for the dynamics of superparamagnetic nanoparticles interacting with cargoes transported by kinesins. Nonlinear Dynamics. 2017 July 21.
56. Nakata K, Hu Y, Uzun O, Bakr O, Stellacci F. Chains of Superparamagnetic Nanoparticles. Advanced Materials. 2008;20(22):4294-9.
57. Gonzalez-Moragas L, Yu S-M, Benseny-Cases N, Stürzenbaum S, Roig A, Laromaine A. Toxicogenomics of iron oxide nanoparticles in the nematode C. elegans. Nanotoxicology. 2017 2017/05/28;11(5):647-57.
58. Gonzalez-Moragas L, Yu S-M, Carenza E, Laromaine A, Roig A. Protective Effects of Bovine Serum Albumin on Superparamagnetic Iron Oxide Nanoparticles Evaluated in the Nematode Caenorhabditis elegans. ACS Biomaterials Science & Engineering. 2015 2015/11/09;1(11):1129-38.
59. Lim D, Roh JY, Eom HJ, Choi JY, Hyun J, Choi J. Oxidative stress-related PMK-1 P38 MAPK activation as a mechanism for toxicity of silver nanoparticles to reproduction in the nematode Caenorhabditis elegans. Environmental toxicology and chemistry. 2012 Mar;31(3):585-92. PubMed PMID: 22128035. Epub 2011/12/01. eng.
60. Pluskota A, Horzowski E, Bossinger O, von Mikecz A. In Caenorhabditis elegans Nanoparticle-Bio-Interactions Become Transparent: Silica-Nanoparticles Induce Reproductive Senescence. PLOS ONE. 2009;4(8):e6622.
61. Yang Y-F, Lin Y-J, Liao C-M. Toxicity-based toxicokinetic/toxicodynamic assessment of bioaccumulation and nanotoxicity of zerovalent iron nanoparticles in Caenorhabditis elegans. International Journal of Nanomedicine. 2017 06/26;12:4607-21. PubMed PMID: PMC5500513.
62. Donkin SG, Williams PL. Influence of developmental stage, salts and food presence on various end points using Caenorhabditis Elegans for aquatic toxicity testing. Environmental toxicology and chemistry. 1995;14(12):2139-47.
63. Beron C, Vidal-Gadea AG, Cohn J, Parikh A, Huong G, Pierce-Shimomura JT. The burrowing behavior of the nematode Caenorhabditis elegans: A new assay for the study of neuromuscular disorders. Genes, brain, and behavior. 2015;14(4):357-68. PubMed PMID: PMC4444045.
64. Hart AC. Behavior. 2006. In: WormBook : the online review of C elegans biology [Internet]. The C. elegans Research Community.
65. Gray JM, Hill JJ, Bargmann CI. A circuit for navigation in Caenorhabditis elegans. Proceedings of the National Academy of Sciences of the United States of America. 2005 March 1, 2005;102(9):3184-91.
66. Li W, Feng, Z., Sternberg, P. W., Xu, X. Z. A C. elegans stretch receptor neuron revealed by a mechanosensitive TRP channel homologue. Nature. 2006 Mar 30;440(7084):684-7. PubMed PMID: 16572173. Pubmed Central PMCID: PMC2865900.
67. Wen Q, Po, M., Hulme, E., Chen, S., Liu, X., Kwok, S., Gershow, M., Leifer, A.M., Butler, V., Fang-Yen, C., Kawano, T., Schafer, W. R., Whitesides, G., Wyart, M., Chklovskii, D. B., Zhen, M., Samuel, A. D. T. Proprioceptive coupling within motor neurons drives C. elegans forward locomotion. Neuron. 2012;76(4):750-61. PubMed PMID: PMC3508473.
68. Zablotskii V, Syrovets T, Schmidt ZW, Dejneka A, Simmet T. Modulation of monocytic leukemia cell function and survival by high gradient magnetic fields and mathematical modeling studies. Biomaterials. 2014 Mar;35(10):3164-71. PubMed PMID: 24439412. Epub 2014/01/21. eng.

69. Hughes S, McBain S, Dobson J, El Haj AJ. Selective activation of mechanosensitive ion channels using magnetic particles. J R Soc Interface. 2008 Aug 06;5(25):855-63. PubMed PMID: 18077244. Pubmed Central PMCID: PMC2495030. Epub 2007/12/14. eng.
70. Sensenig R, Sapir Y, MacDonald C, Cohen S, Polyak B. Magnetic nanoparticle-based approaches to locally target therapy and enhance tissue regeneration in vivo. Nanomedicine (London, England). 2012;7(9):1425-42. PubMed PMID: PMC3543693.
71. Wahajuddin, Arora S. Superparamagnetic iron oxide nanoparticles: magnetic nanoplatforms as drug carriers. International Journal of Nanomedicine. 2012 07/06;7:3445-71. PubMed PMID: PMC3405876.

Caenorhabditis elegans locomotion dynamics is affected by internally localized magnetic fields

Eleni Gourgou[1,2,*], Yang Zhang[3,4], Ehsan Mirzakhalili[1], Bogdan Epureanu[1,+]

1. Mechanical Engineering, University of Michigan, Ann Arbor, MI, United States
2. Internal Medicine, Division of Geriatrics, Medical School, University of Michigan, Ann Arbor, MI, United States
3. Electrical Engineering and Computer Science, University of Michigan, Ann Arbor, MI, United States
4. University of Michigan and Shanghai Jiao Tong University Joint Institution, Shanghai, China
* E.G. current address: Mechanical Engineering, University of Michigan, Ann Arbor, MI, United States
+ corresponding author: Bogdan Epureanu, epureanu@umich.edu

Supplementary Information

The features of the magnetic field (MF) presented here are independent of the magnetic particles and depend only on the properties of the electromagnets and the geometry of the setup. However, the forces that are exerted on the particles depend also on the properties of the particle. We have used several different magnetic particles in our experiments. The numerical simulations and analysis are performed only on the largest magnetic particles since such analysis provide us with the largest forces that can be created because of the external MF. Moreover, the characteristics of Dynabeads are more accessible (1) compared to the rest of the particles used in our experiments.

The forces on a magnetic particle in an external MF can be characterized as(2):

$$\mathbf{F} = \rho V \nabla(\mathbf{M}_0 \cdot \mathbf{B}) + \frac{V \chi_{bead}}{\mu_0}(\mathbf{B}.\nabla)\mathbf{B}\ , \qquad [1]$$

where ρ, V, M_0, χ_{bead} are the density, volume, initial magnetization, and initial magnetic susceptibility of the particles, respectively. $\mathbf{F}$ is the force acting on the particle, $\mathbf{B}$ is the external MF, and μ_0 is the permeability of vacuum.

Equation [1] is used with the properties of the magnetic particles (1) and the simulation results from COMSOL Multiphysics for the external MF to calculate the forces acting on the magnetic particles. Figure 2 shows that the magnitude of the force at all locations on the plate, which, as expected, can be observed to be larger near the electromagnets where the MF and its gradient are larger.

The magnetization of the particles creates local modifications to the MF compared to the externally applied MF. From classical physics, the MF around a magnetic dipole can be expressed as:

$$\mathbf{B}(\mathbf{r}) = \frac{\mu_0}{4\pi}\left(\frac{3\mathbf{r}(\mathbf{M}\cdot\mathbf{r})}{r^5} - \frac{\mathbf{M}}{r^3}\right), \qquad [2]$$

where $\mathbf{r}$ is position vector relative to the particle at which the MF is calculated and $\mathbf{M}$ is the magnetic moment of the particle that can be calculated as (2):

$$\mathbf{M} = \mathbf{M}_0 + \frac{\chi_{bead}}{\rho}\frac{\mathbf{B}_{external}}{\mu_0}\ . \qquad [3]$$

Equation [3] is used with the properties of the largest particles in our experiments (1) along with the external MF ($\mathbf{B}_{external}$) created by the electromagnets obtained from COMSOL Multyphysics to determine the magnetic moments of the particles in the presence of the external MF. Next Eq. [2] is used to calculate the MF around the particles when the magnetic moment is known. Figure 3 shows the magnitude of the MF flux for vertical and horizontal configuration of three magnetic particles using Eqs. [2] and [3] in MATLAB. The MF is strong close to the particles for both configurations, and decays rapidly with distance from the particles.

The MF shown in Figure 3 can also be used to calculate the gradient of the MF around the particles. Figure 3 show the gradient of the magnetic of for both horizontal and vertical configuration. Again, the gradient of the MF is strongest near the particles and decays rapidly with distance from the particles.

Finally, the forces between two magnetic particles can be found as (3):

$$\mathbf{F}_{12} = -\frac{3\mu_0 M^2}{4\pi r_{12}^{\ 4}}\left(-(\mathbf{n}_1 \cdot \mathbf{n}_2)\mathbf{t}_{12} - (\mathbf{n}_2 \cdot \mathbf{t}_{12})\mathbf{n}_1 - (\mathbf{n}_1 \cdot \mathbf{t}_{12})\mathbf{n}_2 + 5(\mathbf{n}_1.\mathbf{t}_{12})(\mathbf{n}_2.\mathbf{t}_{12})\mathbf{t}_{12}\right) \quad [4]$$

where $\mathbf{F}_{12}$ is the force between the two particles, r_{12} is the distance between the two particles, $\mathbf{t}_{12}$ is the unit vector that connects the two particles , $\mathbf{n}_1$ and $\mathbf{n}_2$ are the direction of the magnetic moment for particle 1 and 2, and M is the magnitude of the magnetic moment of the two particles. Here, we have assumed that the distance between the two particles is small leading to the same magnetic moment for both particles based on Eq. [3]. Figure 3E shows how the force between two particles changes for both vertical and horizontal direction. The force between the particles in the horizontal direction is repulsive while the force between the particles in the vertical direction is attractive. The attractive forces between the particles cause them to form chain-like structures when they are not interrupted by the medium in which the particles are located (3, 4).

References

1. Fonnum G, Johansson C, Molteberg A, Mørup S, Aksnes E. Characterisation of Dynabeads® by magnetization measurements and Mössbauer spectroscopy. Journal of Magnetism and Magnetic Materials. 2005;293(1):41-7.
2. Shevkoplyas SS, Siegel AC, Westervelt RM, Prentiss MG, Whitesides GM. The force acting on a superparamagnetic bead due to an applied magnetic field. Lab Chip. 2007;7(10):1294-302.
3. Mirzakhalili E, Nam W, Epureanu BI. Reduced-order models for the dynamics of superparamagnetic nanoparticles interacting with cargoes transported by kinesins. Nonlinear Dynamics. 2017.
4. Nakata K, Hu Y, Uzun O, Bakr O, Stellacci F. Chains of Superparamagnetic Nanoparticles. Advanced Materials. 2008;20(22):4294-9.

Figure 1

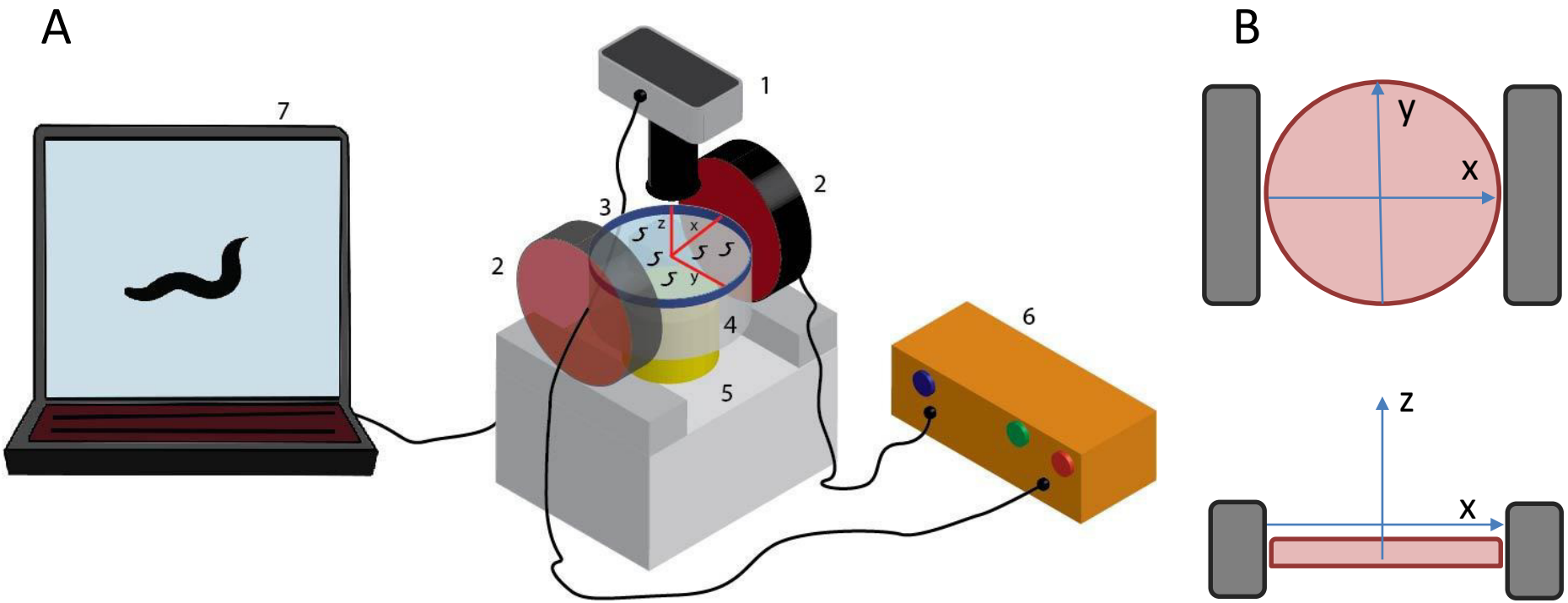

Figure 1: A: Experimental set up for the application of gradient magnetic field on freely moving *C. elegans.* 1: Objective lens and camera; 2: Electromagnets; 3: NGM plate with freely moving *C. elegans,* with schematic of plate orientation, red lines indicating the x and y axes ; 4: Auxiliary transparent base; 5: Working stage with bright light source; 6: Power supply; 7: Computer and recording software. Objects are not depicted at scale. B: Schematic of the orientation of the NGM plate (pink circle), *x*, *y* and *z* axes, and electromagnets (grey rectangles), top: view from above, bottom: view from a side.

Figure 2

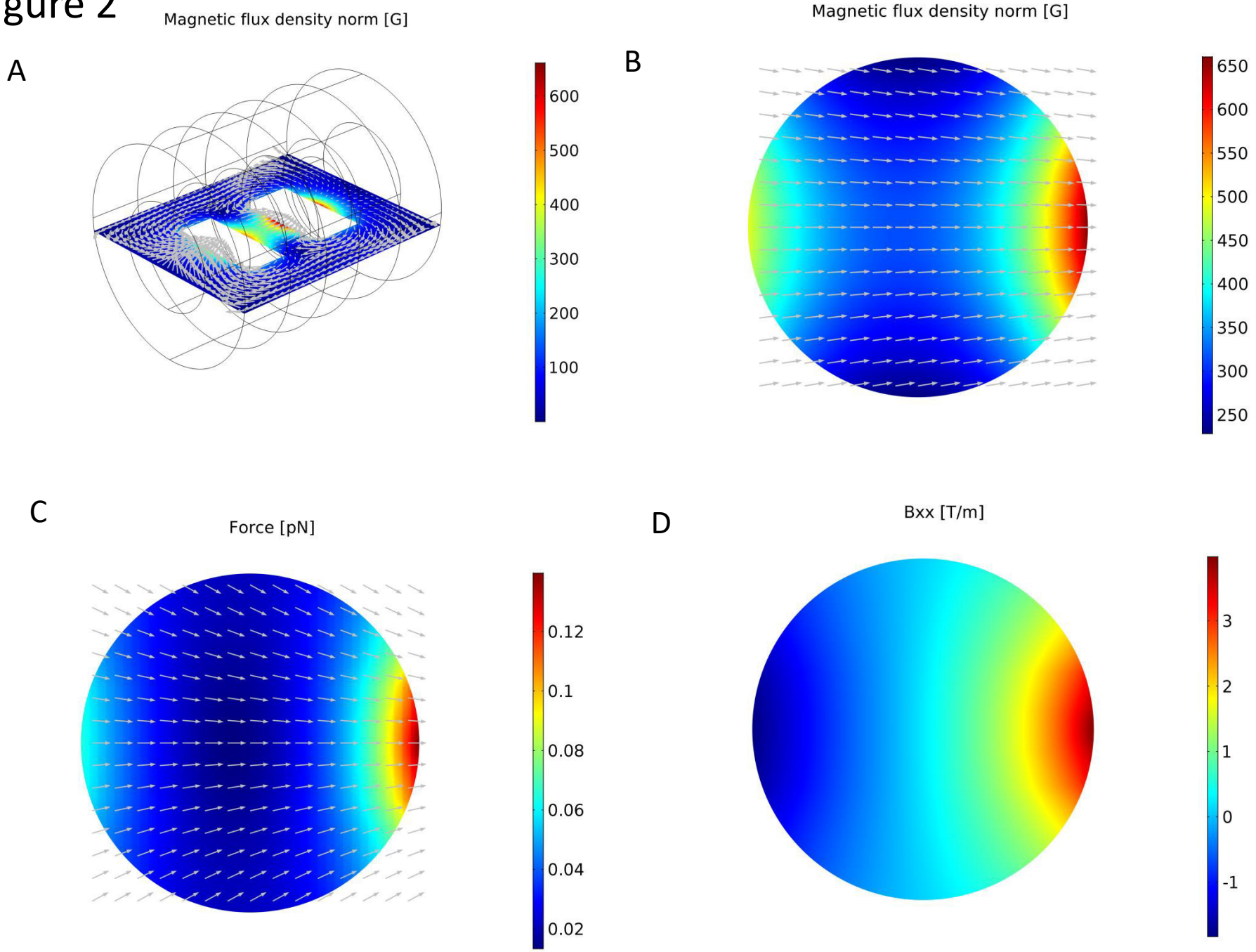
A
Magnetic flux density norm [G]
600
500
400
300
200
100
B
Magnetic flux density norm [G]
650
600
550
500
450
400
350
300
250
C
Force [pN]
0.12
0.1
0.08
0.06
0.04
0.02
D
Bxx [T/m]
3
2
1
0
-1

Figure 2: COMSOL Multiphysics simulation results for the magnetic field generated by the electromagnets. A: Overview of the magnetic field flux density on the plane of the worm plate surface. The arrows show the direction of the magnetic flux. B: The magnetic field flux density distribution on the worm plate surface. The arrows indicate the direction of the magnetic field (the component of the magnetic field in the perpendicular direction is set equal to zero to avoid arrows going in/out of the plane). C: The magnetic forces applied on particles located on the plane of the worm plate surface. The arrows show the direction of the magnetic forces (the component of the force in the perpendicular direction is set equal to zero to avoid arrows going in/out of the plane). D: The gradient of the magnetic field in the direction of the axis that connects the centers of the two electromagnets.

Figure 3

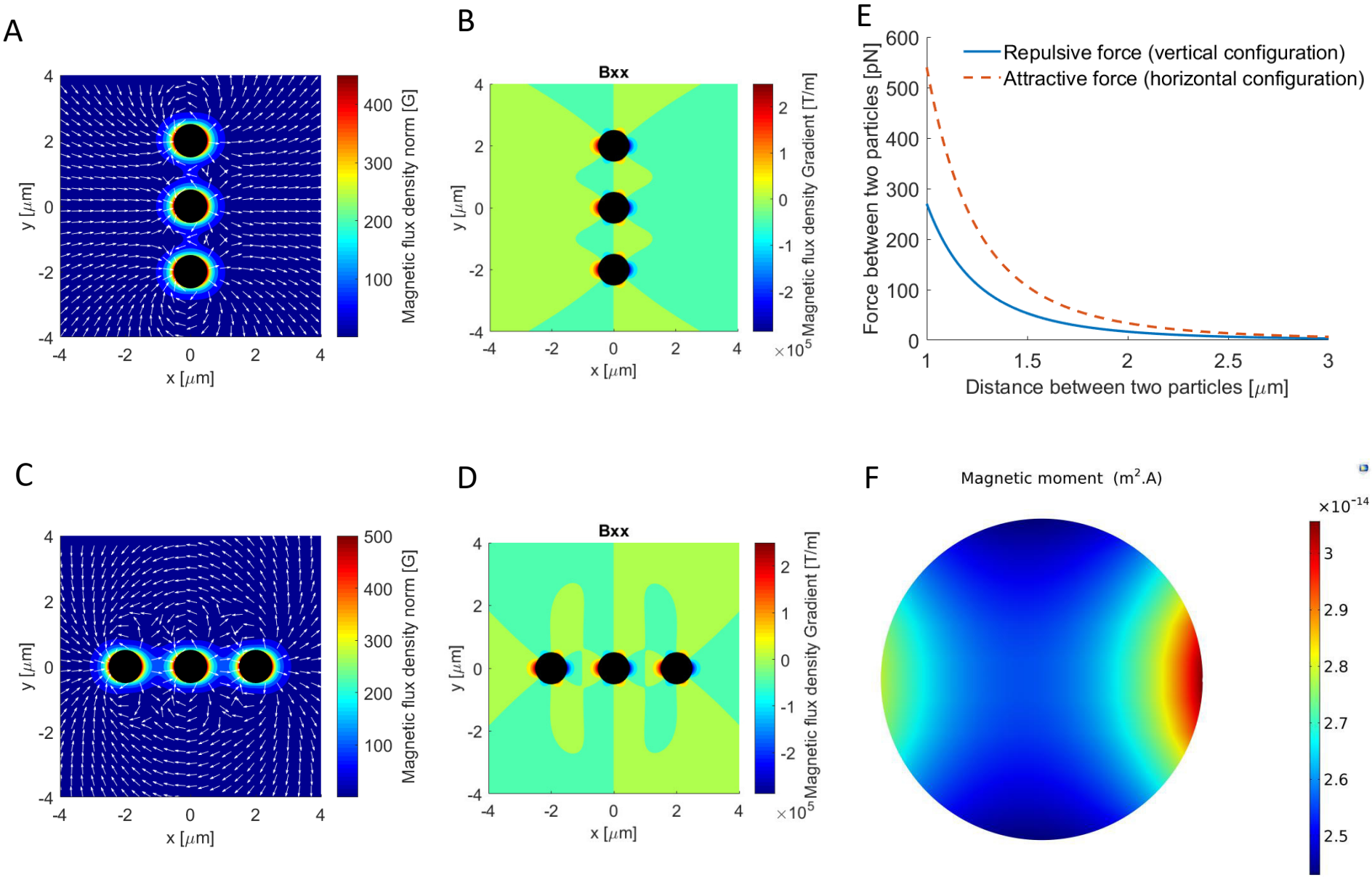
A
y [μm]
x [μm]
Magnetic flux density norm [G]
B
Bxx
y [μm]
x [μm]
Magnetic flux density Gradient [T/m]
×10^5
E
Repulsive force (vertical configuration)
Attractive force (horizontal configuration)
Force between two particles [pN]
Distance between two particles [μm]
C
y [μm]
x [μm]
Magnetic flux density norm [G]
D
Bxx
y [μm]
x [μm]
Magnetic flux density Gradient [T/m]
×10^5
F
Magnetic moment (m^2.A)
×10^-14

Figure 3: Characterization of the magnetic field around the 1μm nanoparticles for two different configurations. The direction of magnetic moment for both configurations is along the x axis, as is shown in Fig. 1. The magnetic moment of the particles is assumed to be similar and equal to the maximum value that is computed from the COMSOL Multiphysics simulations in the plate. A: The magnetic field flux density around three magnetic particles in the configuration along the y axis. The arrows indicate the direction of the magnetic field. B: The largest component of the gradient of the magnetic field for the configuration of the magnetic particles along the y axis. C: The magnetic field flux density norm around three magnetic particles in the configuration along the x axis. The arrows indicate the direction of the magnetic field. D: The largest component of the gradient of the magnetic field for the configuration of the magnetic particles along the x axis. E: The forces between two particles in each configuration. F: The magnetic moment of the external magnetic field, which the particles experience once inside the magnetic field.

Table 1

Group	Particle Size	Coating	Magnetic properties	Fluorescence
Group C	-	-	-	-
Group 1	1 µm	Streptavidin	Superparamagnetic, iron core	No
Group 100	100 nm	No	Magnetic, dextran iron oxide composite	Rhodamine
Group 40	40 nm	-COOH	Magnetic, iron oxide (magnetite)	No

Table 1: Groups of worms tested and properties of the respective nanoparticles.

Figure 4

A

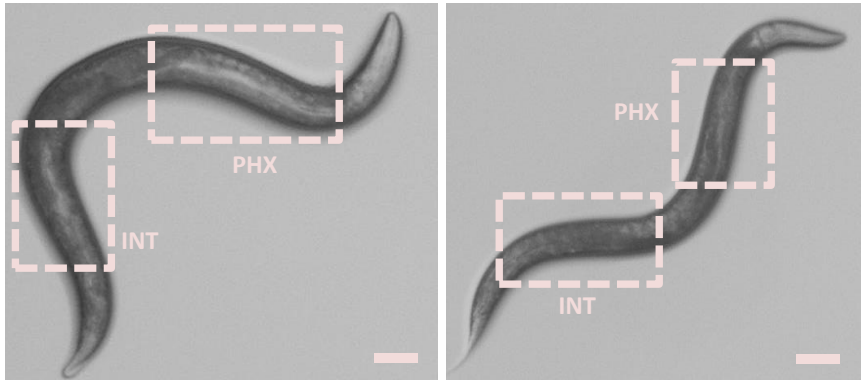

Group C Group 1

B

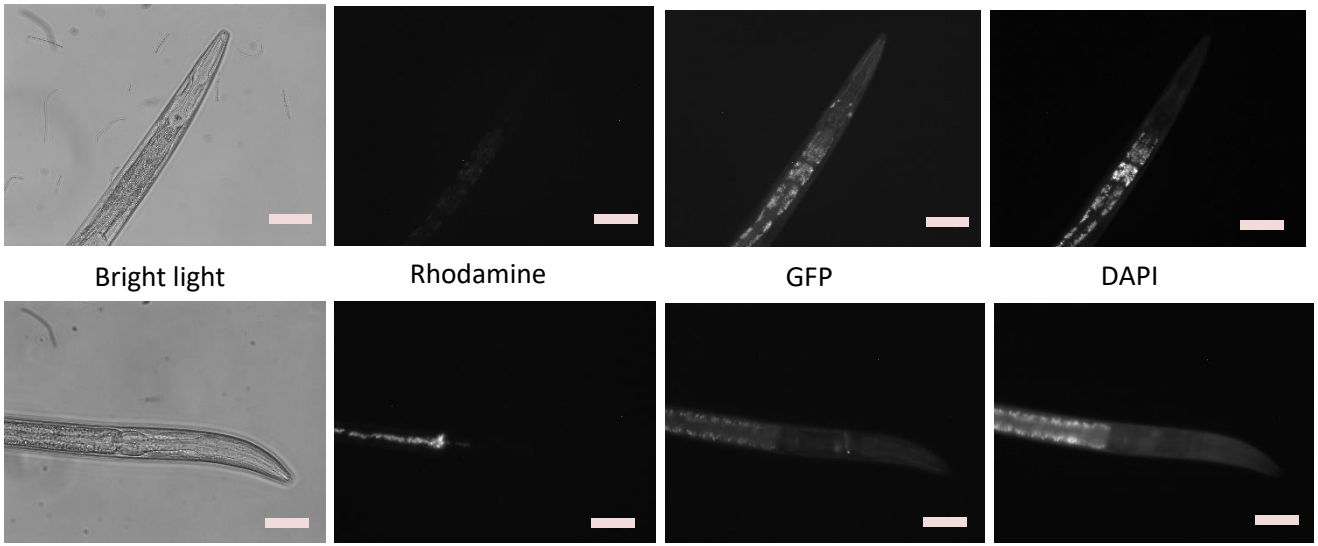

Bright light Rhodamine GFP DAPI

Group C

Group 100

C

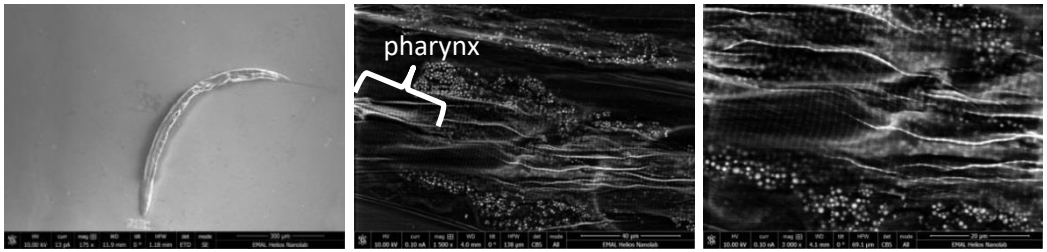

Group 40 Group 40

Figure 4: Confirmation of nanoparticles uptake in young adult *C. elegans*. A) Internalization of 1µm magnetic particles is verified by bright field microscopy. Left: worm fed with plain *E. coli* OP50 (control, Group C). Right: worm fed with *E. coli* OP50 mixed with 1µm particles. Particles appear to be aggregated in the dark-colored pharynx (PHX) and intestine (INT) of Group 1 worms, in contrast to the light-colored pharynx (PHX) and intestine (INT) of Group C worms. Scale bar: 0.1mm. B) Internalization of 100nm magnetic, fluorescent nanoparticles is verified by epifluorescent microscopy. Top panels: worm fed with plain *E. coli* OP50 (control, Group C), bottom panels: worm fed with E. coli OP50 mixed with 100nm particles. Bright light: worms illuminated by bright light source; rhodamine: worms visualized with optical filter for rhodamine, Excitation 545nm/Emission 565nm; GFP: worms visualized with optical filter for green fluorescent protein (GFP), Excitation 395nm/Emission 510nm; DAPI: worms visualized with optical filter for DAPI, Excitation 358nm/Emission 460nm. In GFP and DAPI images, autofluorescence is the only fluorescence detected. Scale bar: 0.1mm. C). Internalization of 40nm magnetic particles is verified by scanning electron microscopy (SEM). Left: a whole *C. elegans* as captured by SEM, using Everhart-Thornley SE detector. Center: 40 nm particles, shown as white dots, detected close to *C. elegans* pharynx, using circular backscatter (CBS) detector, magnification 1500x. Right: 40 nm particles, shown as white dots, detected close to *C. elegans* pharynx, using circular backscatter (CBS) detector, magnification 3000x. Location of particles is approximate, due to distortion generated during sample processing.

Figure 5
Posture Features (A-D)

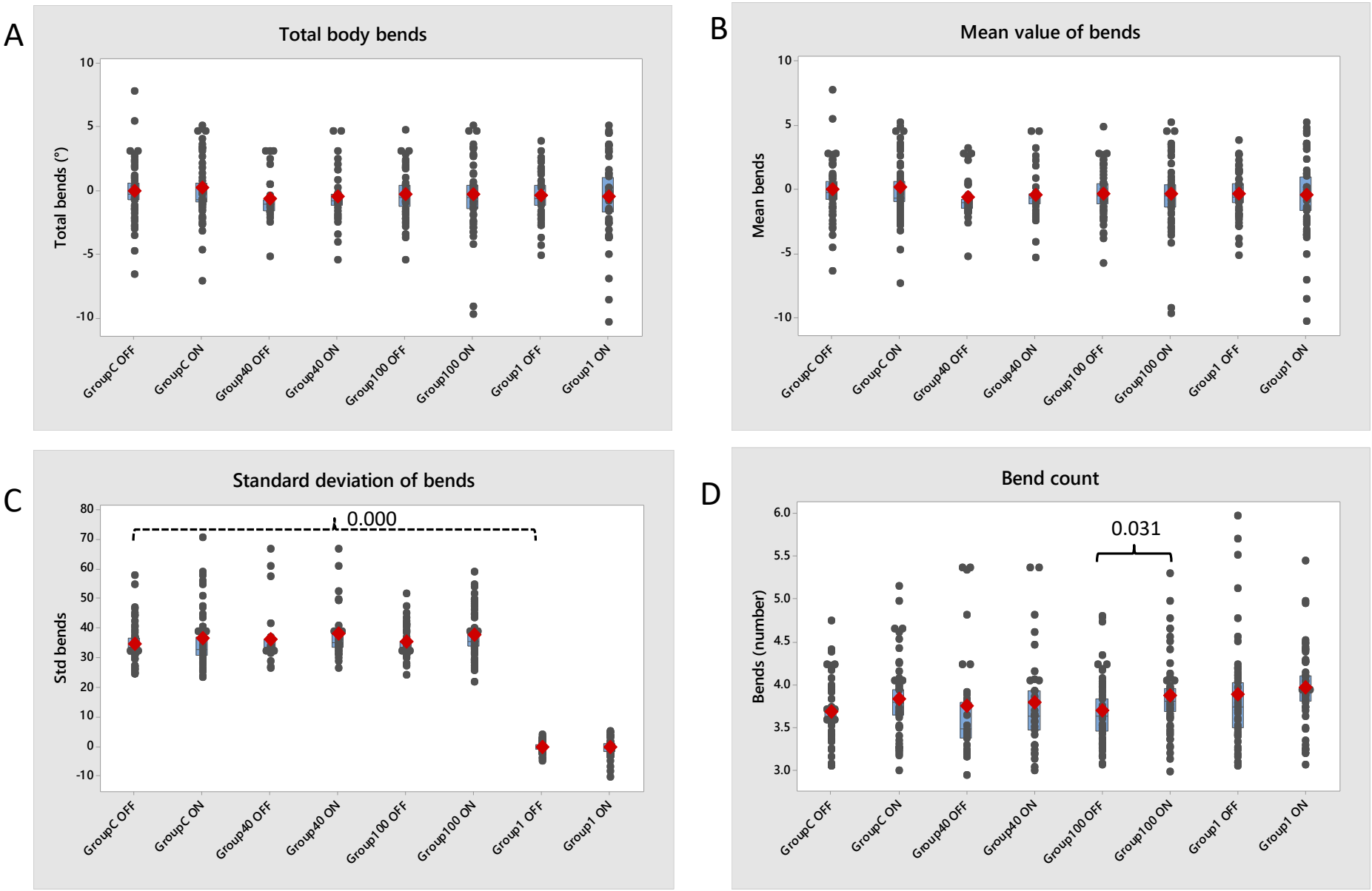

Figure 5 (continued)
Motion Features (E-K)

E

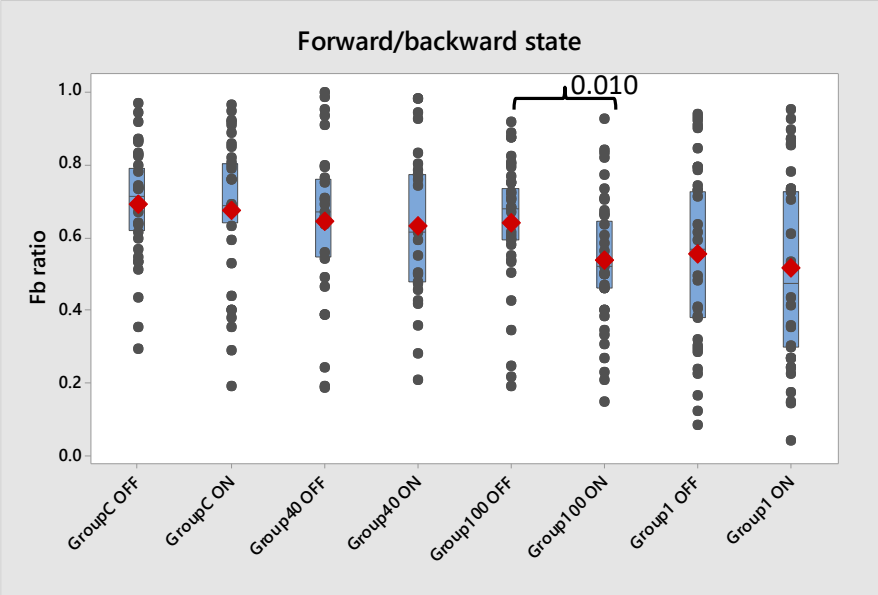

F

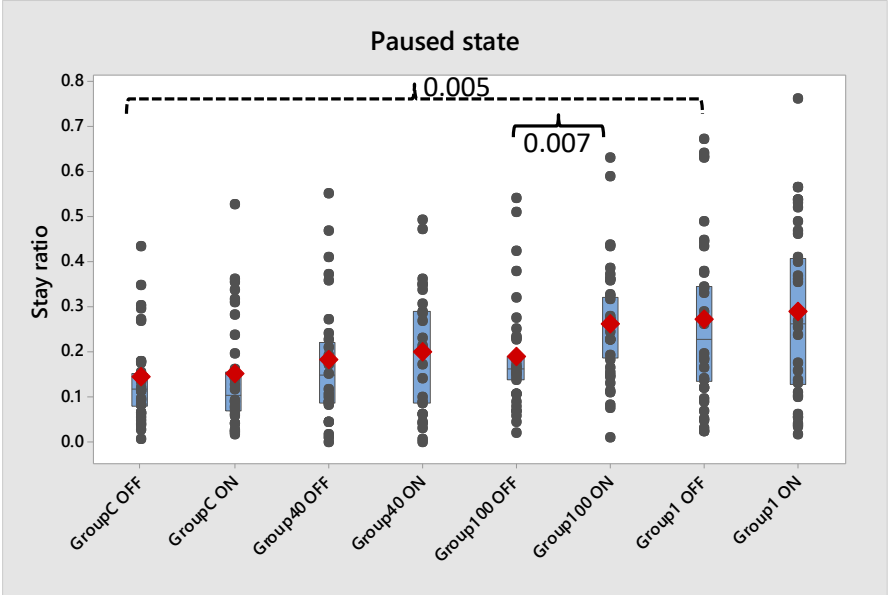

G

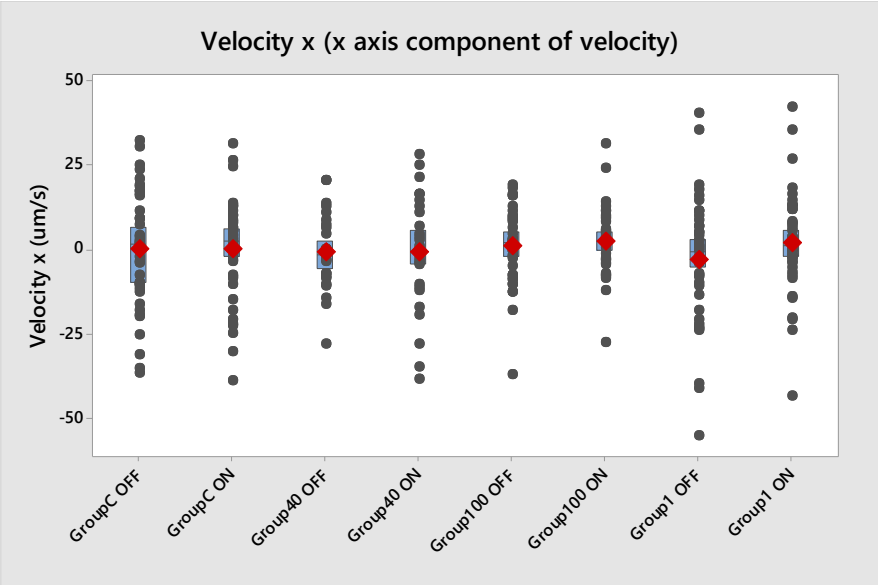

H

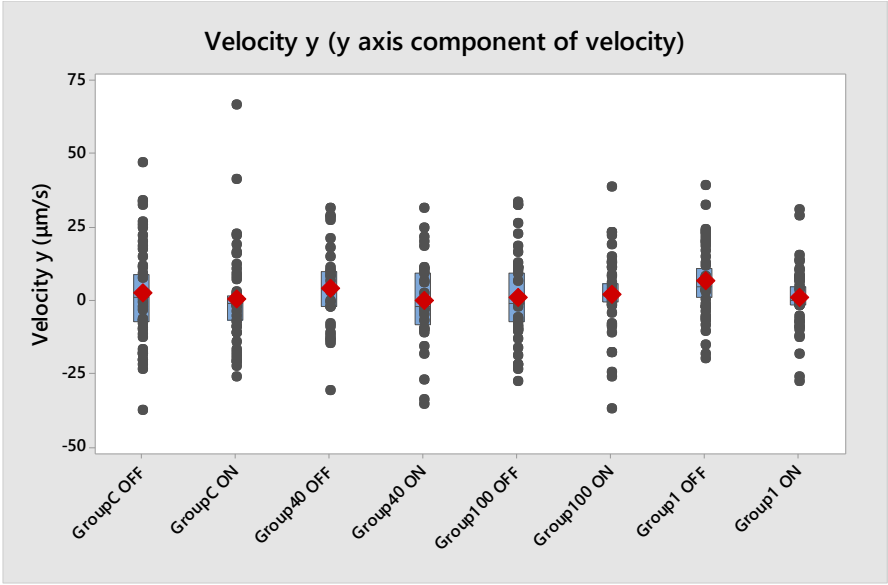

I

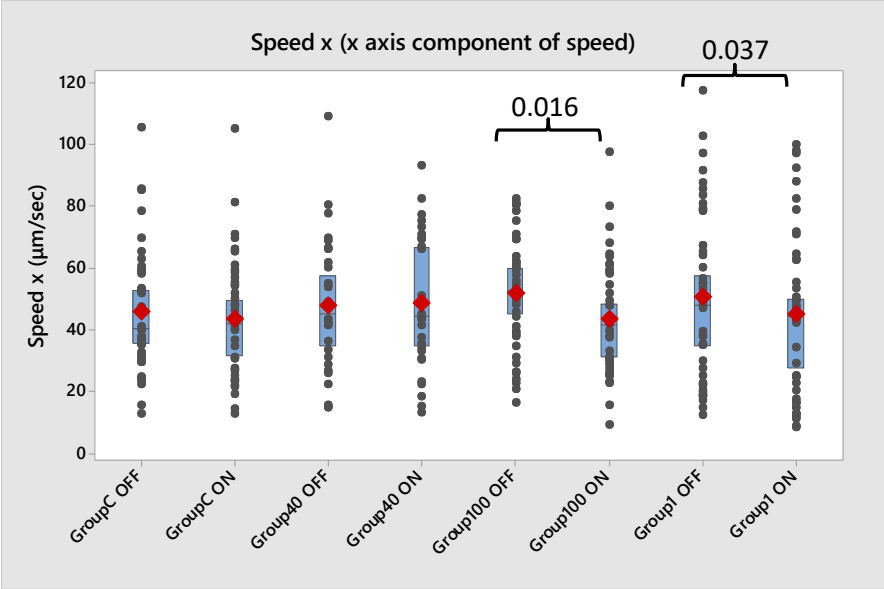
Speed x (x axis component of speed)
0.016
0.037
Speed x (µm/sec)
0
20
40
60
80
100
120
GroupC OFF
GroupC ON
Group40 OFF
Group40 ON
Group100 OFF
Group100 ON
Group1 OFF
Group1 ON

J

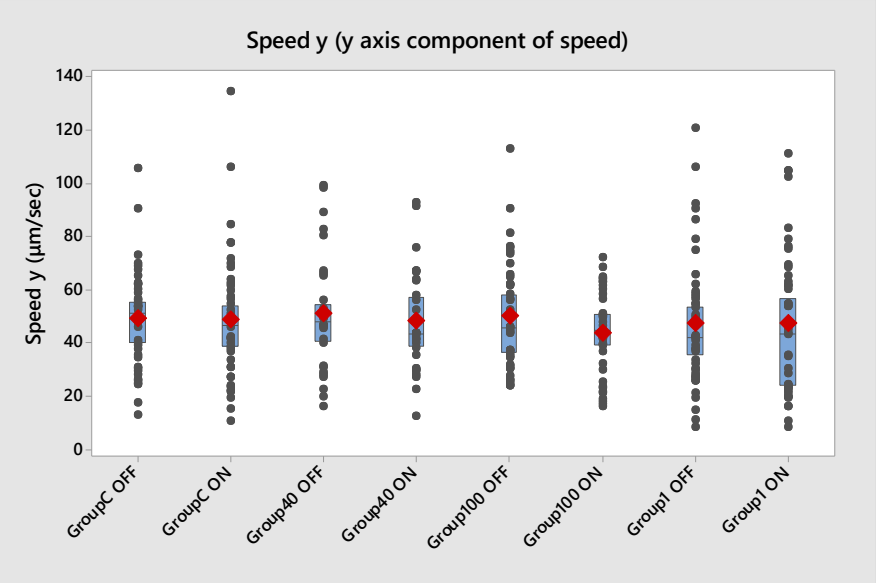
Speed y (y axis component of speed)
Speed y (µm/sec)
0
20
40
60
80
100
120
140
GroupC OFF
GroupC ON
Group40 OFF
Group40 ON
Group100 OFF
Group100 ON
Group1 OFF
Group1 ON

K

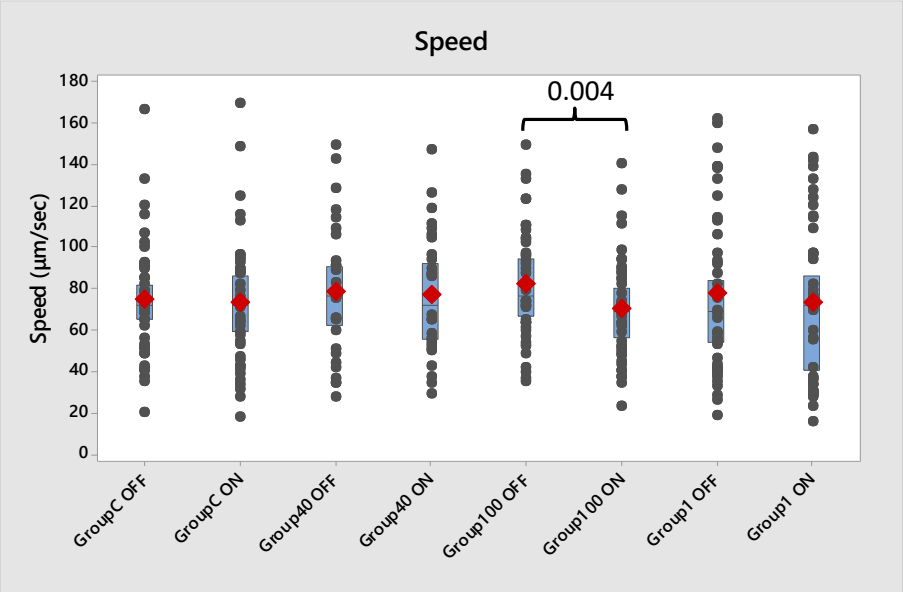
Speed
0.004
Speed (µm/sec)
0
20
40
60
80
100
120
140
160
180
GroupC OFF
GroupC ON
Group40 OFF
Group40 ON
Group100 OFF
Group100 ON
Group1 OFF
Group1 ON

Figure 5 (continued)
Path Features (L-O)

L

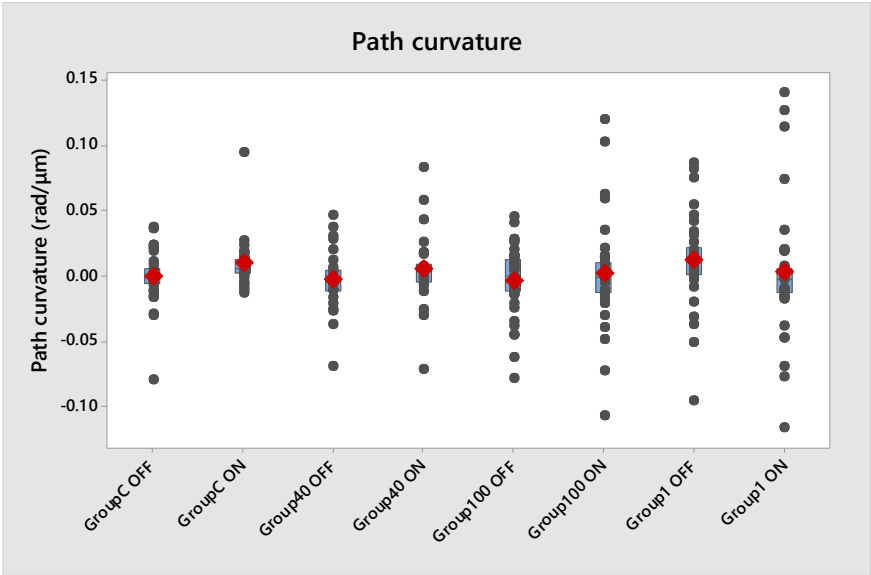

M

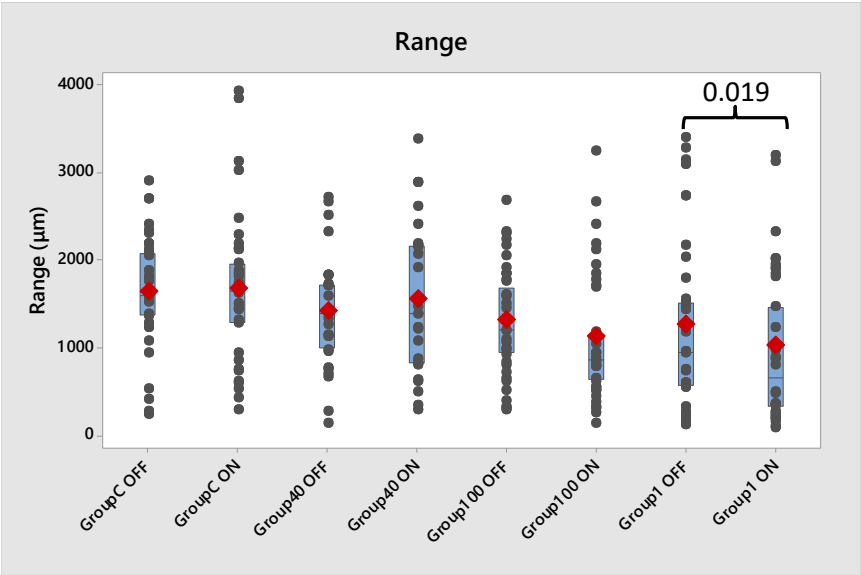

N

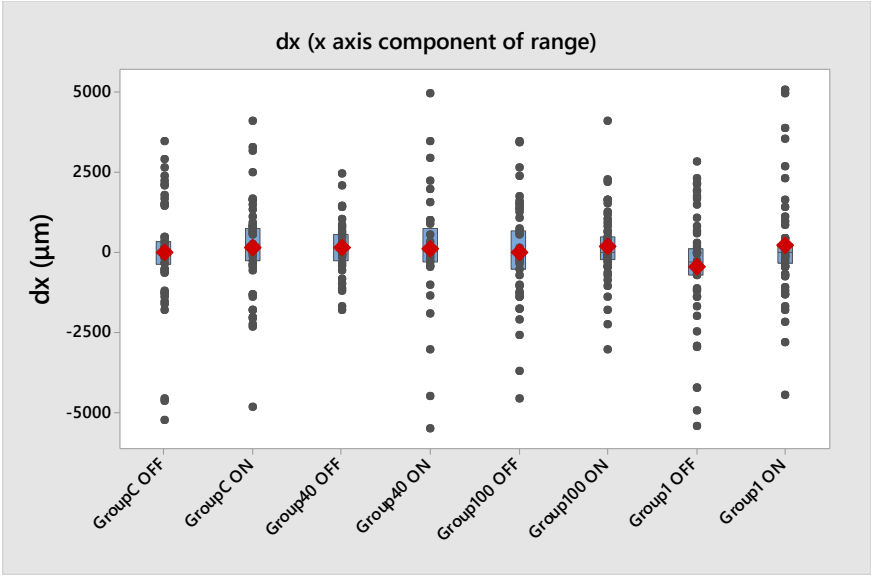

O

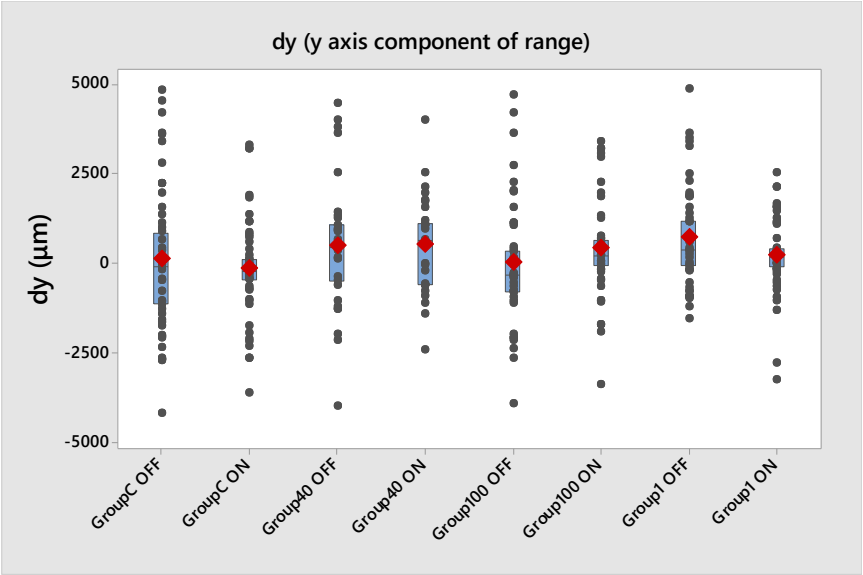

Figure 5: Locomotion features and their metrics, as they have been quantified for all four groups of worms tested (Group C: control animals, fed on plain food source *E. coli* OP50; Group 1: fed on *E. coli* OP50 mixed with 1 μm-diameter superparamagnetic particles; Group 100: fed on *E. coli* OP50 mixed with 100nm-diameter iron core paramagnetic particles, and Group 40: fed on *E. coli* OP50 mixed with 40nm-diameter iron core paramagnetic particles) in the absence (OFF state) or in the presence (ON state) of external magnetic field. A-D: Posture features, E-K: Motion features, L-O: Path features. For each group tested, 29-42 worms were tracked in 3 different experimental days. Grey dots represent individual worms; red diamonds represent the mean; blue boxes indicate the median confidence interval box, with a middle line indicating the median. Dashed lines show comparisons between worms of different groups in the absence of magnetic field (OFF state). Continuous lines show comparisons between the ON and OFF state of worms of the same group. All p-values given are calculated by the Wilcoxon Signed Rank test with confidence interval set at 95%, and any difference was considered statistically significant when $p \leq 0.05$. The p-values for all comparisons are given in Tables S1 and S2.

Supplementary Figures and Tables

Supplementary Figure S1

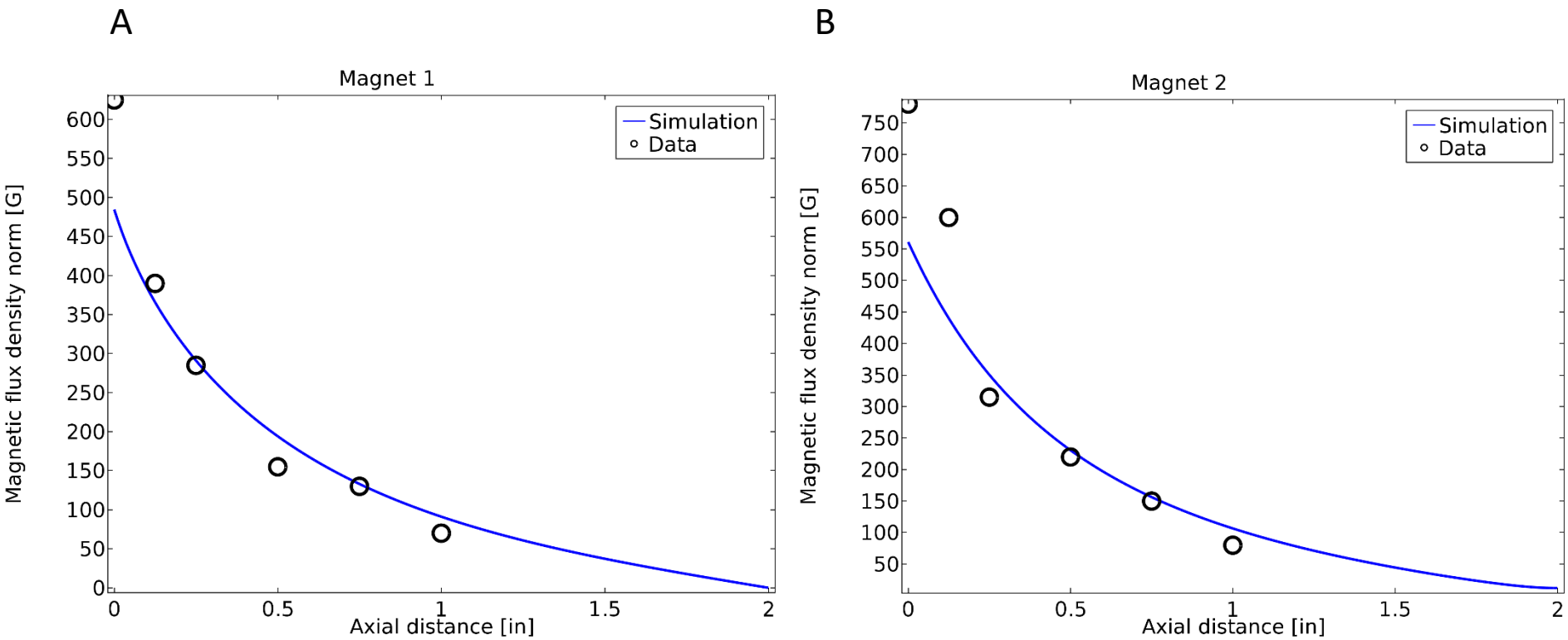

Figure S1: Calibration of the parameters in COMSOL Multiphysics simulations to match the available data for magnet 1 (A) and magnet 2 (B) that are used in the experiments.

Supplementary Figure S2

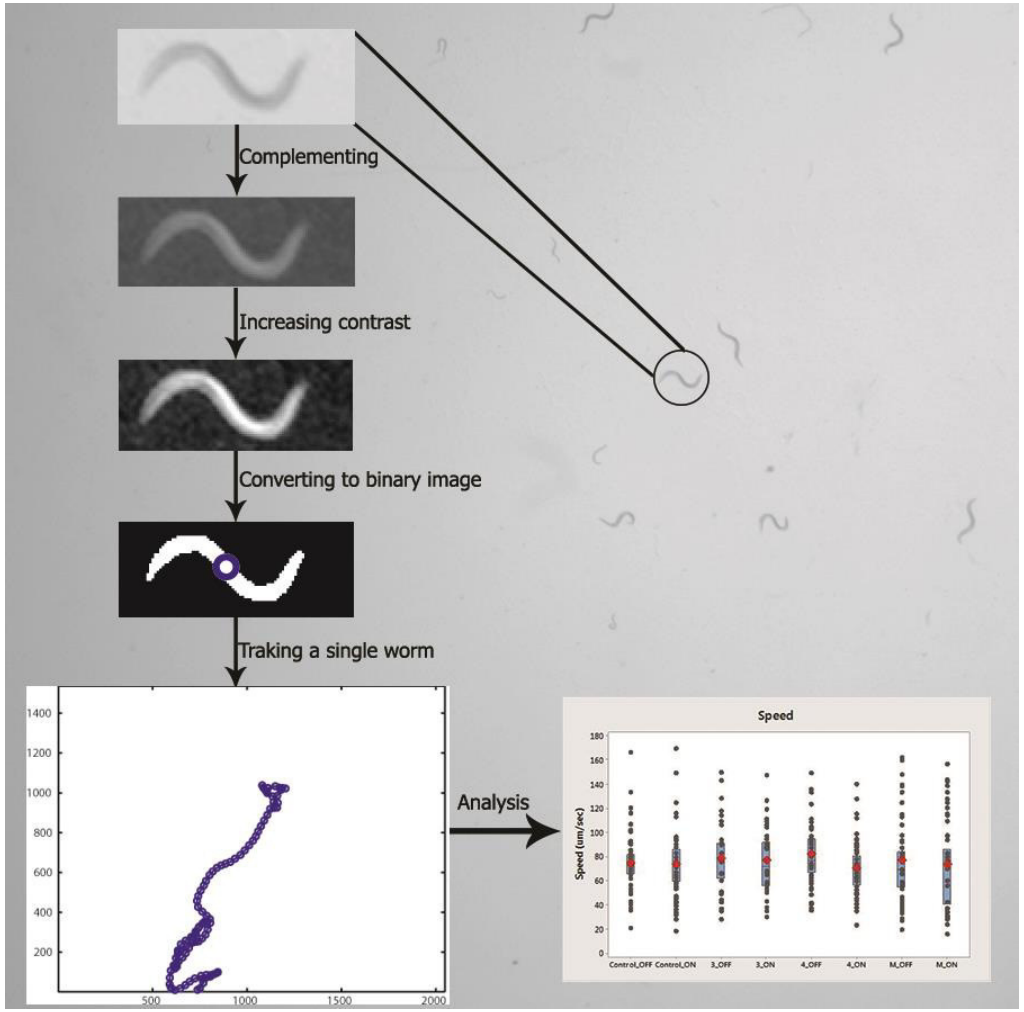

Figure S2: An overview of the steps that are taken to analyze the locomotion of the worms. First, a worm is selected in the first frame to be tracked. Next, several image enhancements are performed on the subframe that is created around the selected worm. Next, the grayscale image is converted to a binary image and the postprocessing such as finding the centroid of the worm is performed. All these steps are conducted for the whole movie that is recorded. Finally, the data collected from all experiments are compared.

Supplementary Figure S3

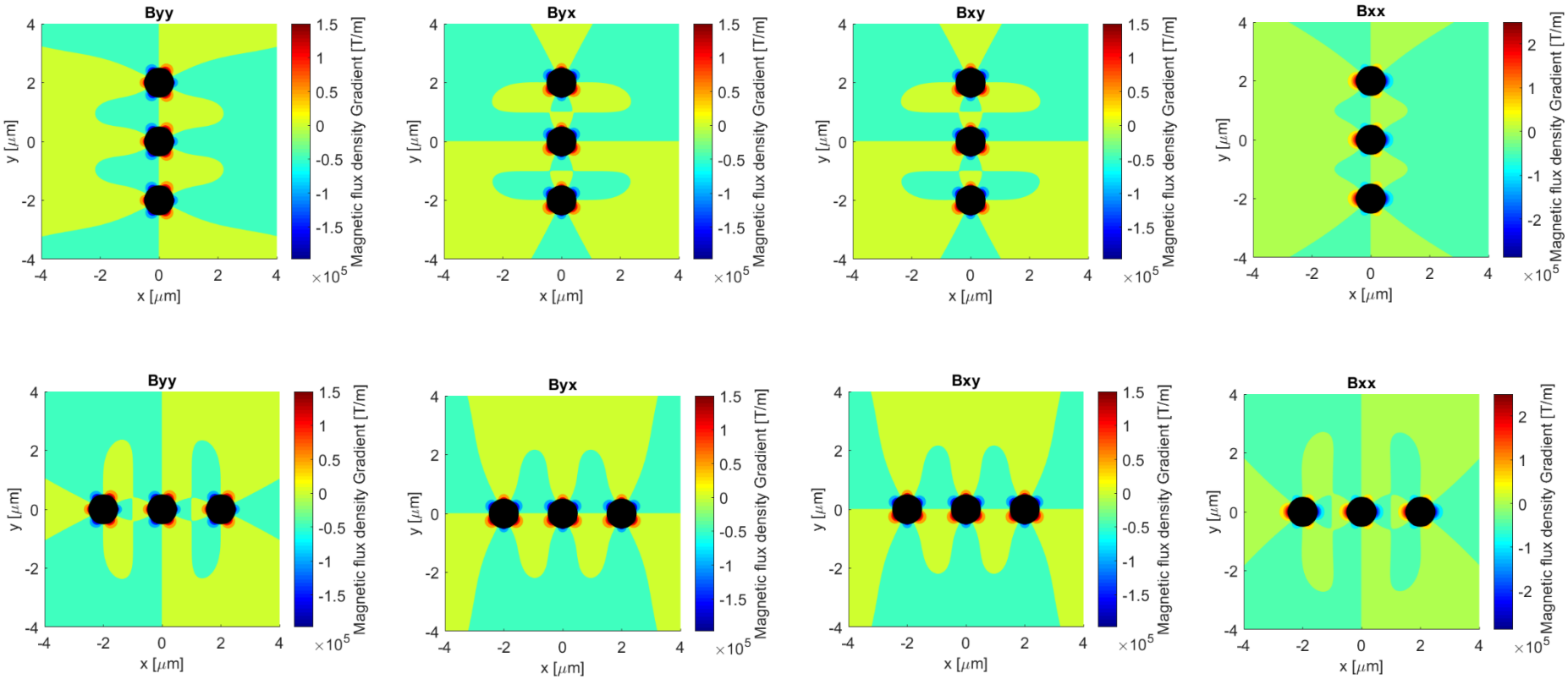

Figure S3: All components of the gradient of the magnetic field for the particles configured along the y axis and along the x axis.

Supplementary Figure S4

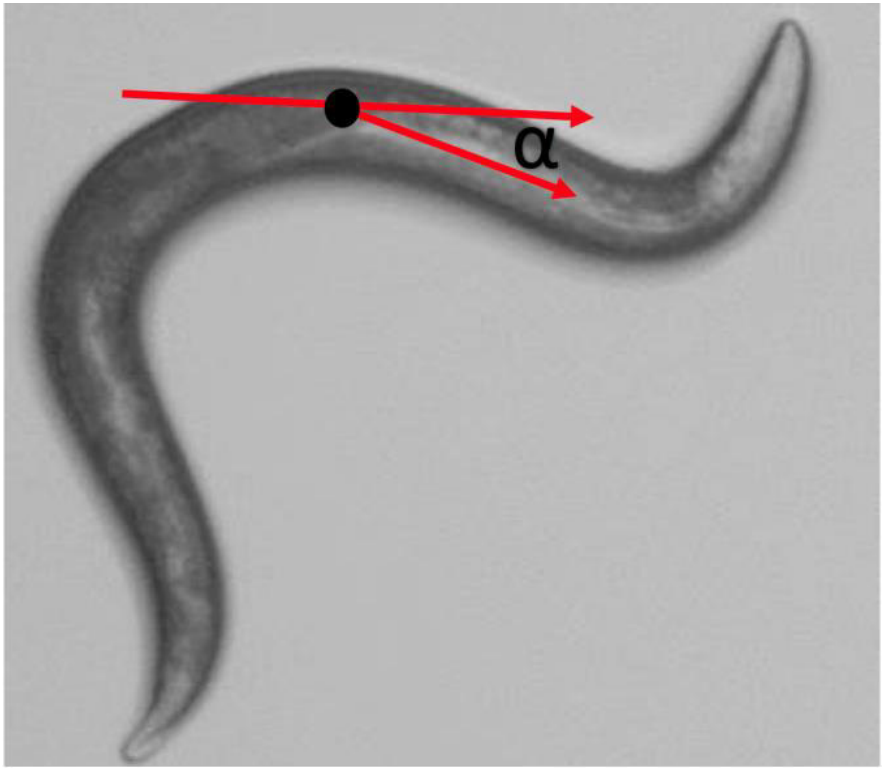

Figure S4: The supplementary angle α is the difference in tangent angles at each skeleton point

Supplementary Table S1

Metric	Group C OFF/ON	Group 1 OFF/ON	Group 100 OFF/ON	Group 40 OFF/ON
Total bends	0.645	0.645	0.644	0.540
Mean value of bends	0.661	0.696	0.735	0.464
Standard deviation of total bends	0.177	0.645	0.092	0.234
Bend count	0.052	0.093	**0.031**	0.764
Forward/backward ratio	0.681	0.193	**0.010**	0.747
Stay ratio	0.967	0.336	**0.007**	0.706
Velocity x	0.832	0.375	0.477	0.979
Velocity y	0.599	0.066	0.514	0.375
Speed x	0.431	**0.037**	**0.016**	0.936
Speed y	0.235	0.066	0.093	0.435
Speed	0.438	0.190	**0.004**	0.554
Path curvature	0.120	0.059	0.543	0.225
Range	0.773	**0.019**	0.104	0.706
dx	0.960	0.280	0.499	0.914
dy	0.626	0.250	0.217	0.920

Table S1: The magnetic field effect on the locomotion of worms with internalized nanoparticles. P-values of Wilcoxon Signed Rank test for all comparisons between OFF and ON state of each group studied. With bold are highlighted the statistically significant differences, with $p \leq 0.05$.

Supplementary Table S2

Metric	Kruskal-Wallis	Group C vs Group 1	Group C vs Group 100	Group C vs Group 40
Total bends	0.649			
Mean value of bends	0.618			
Standard deviation of total bends	**0.000**	**0.000**	0.563	**0.044**
Bend count	0.237			
Forward/backward ratio	0.234			
Stay ratio	**0.045**	**0.005**	0.226	0.064
Velocity x	0.729			
Velocity y	0.321			
Speed x	0.498			
Speed y	0.804			
Speed	0.661			
Path curvature	0.096			
Range	0.115			
dx	0.649			
dy	0.188			

Table S2: The particle effect on the locomotion of worms with internalized nanoparticles. The second column shows the p-values of Kruskal-Wallis test used to compare all groups of worms studied during their OFF state. The last three columns show the p-values of the Wilcoxon Signed Rank test used to compare Group C with each of the other three particle-containing groups. The Wilcoxon Signed Rank test was run only when Kruskal-Wallis test gave $p \leq 0.05$. With bold are highlighted the statistically significant differences, with $p \leq 0.05$.